Andrea Maria Triebl, Bsc.

Deracemization of *N*-(2-methylbenzylidene)-phenylglycine amide via temperature cycles in a continuous tubular reactor

MASTER'S THESIS

to achieve the university degree of

Diplom-Ingenieurin

Master's degree programme: Chemical Engineering

submitted to

Graz University of Technology

Supervisor
Assoc. Prof. Dipl.-Ing. Dr. techn. Heidrun Gruber-Wölfler

Co-Supervisor
Dipl.-Ing. Dr. techn. Peter Neugebauer, Bsc.

Institute of Process and Particle Technology

Graz, November 2019

AFFIDAVIT

I declare that I have authored this thesis independently, that I have not used other than the declared sources/resources, and that I have explicitly indicated all material which has been quoted either literally or by content from the sources used. The text document uploaded to TUGRAZonline is identical to the present master's thesis.

Date

Signature

Acknowledgements

I would like to thank Assoc. Prof. Dipl.-Ing. Dr. techn. Heidrun Gruber-Wölfler for the supervision of my work. She was a great help and had always time for questions and concerns.

Furthermore, I owe my gratitude to Dipl.-Ing. Dr. techn. Peter Neugebauer, Bsc. He was the driving force in developing the framework of this thesis. Always willing to listen to me, he helped me a lot in establishing the experimental setup and with upcoming problems.

I am also thankful to the other members of the Institute of Process and Particle Technology for the helpful discussions. At this point I would like to emphasize Christoph Neubauer, who helped me to solve many minor problems in the lab.

Last but not least, I would like to thank my parents and my whole family. I am grateful that they always supported my decisions and helped me in all regards.

Abstract

Since the enantiomers of a compound can have different physiological effects on the human body, chirality is an important issue in the pharmaceutical industry. Therefore, the focus is more and more on the production of enantiomerically pure products [1, 2].

This can be achieved directly via adaption of the syntheses so that only the target enantiomer is produced. An example for this is asymmetric catalysis but it often causes complex conditions and low yields [3]. Another option is resolving of racemic mixtures [4]. However, the maximum theoretical yield of separation methods is limited to 50 % as long as there is no additional unit at which the conversion of the undesired to the desired enantiomer takes place [5]. Therefore, Viedma ripening is a promising method, since total resolution of conglomerate forming substances in one step is possible during isothermal wet milling [6, 7]. Another method that is based on similar effects is the temperature cycling technique, at which the crystals in their respective saturated solution are forced to temperature cycles [8].

Due to several advantages, like the faster heat transfer [9, 10, 11], the present master's thesis shows that it is beneficial not to resolve the crystals batch wise but in continuous flow. It has been successfully proven before that crystal properties such as size and shape can be tuned, if pumped through a tube coiled up in two water baths, which are held isothermally at different temperatures [12]. Therefore, in this master's thesis, a similar setup has been used for investigating the deracemization of crystals suspended in their respective saturated solution.

The results of this thesis indicate that the deracemization of *N*-(2-methylbenzylidene)-phenylglycine amide with the catalyst diazabicyclo[5.4.0]undec-7-ene in ethanol is possible in flow. For this purpose, a tubular reactor was used. The experiments were performed with air in a slug flow regime and all experiments were started with a slight enantioimbalance to ensure that each time the same enantiomer was favored. To compare different experiments, the cycle number based deracemization constant k_N and the productivity P were used as conclusive parameters.

Furthermore, the influences of the particle size of the starting material, difference of the water bath temperatures, catalyst amount, residence time and crystal mass were examined. High catalyst amounts and high temperature differences accelerated the deracemization, as long as no nucleation occurred, whereas high pump rates and crystal masses slowed it down. However, high crystal masses and high pump rates increased the productivity as a better yield could be achieved and the total process time could be minimized as the time required per cycle was shorter.

Contents

1 Motivation

Many molecules in nature are chiral, meaning that they have no plane of symmetry [13]. Further, they are called enantiomers, if they can not be superimposed with their mirror image. Since such molecules interact differently in a chiral environment [13], chirality is an important topic in fields like synthetic, food or environmental chemistry, to name only a few [14]. It is obvious that chirality is also especially important in the pharmaceutical industry, as many compounds in living cells are chiral. Since some enantiomers can cause unwanted side effects [13, 15], much effort is taken to produce enantiomerically pure products [1, 2].

Basically, pure products can be obtained if they are already synthesized in a pure way, or the product is purified afterwards [4]. There are many attempts to purify a mixture of two enantiomers. For example, resolution can be achieved via alternate crystallization of the enantiomers (preferential crystallization) [16], or substrate selective reactions (kinetic resolution) [17]. Often, this reactions are performed with enantioselective catalysts or enzymes, which react preferentially with the desired enantiomer and enable separation [18]. Another possibility is the addition of a chiral component, resulting in the formation of diastereomers, which then can be separated [19]. However, a method named Viedma ripening is especially promising [6]. Via Viedma ripening, it is possible to obtain total resolution in only one step during wet milling. However, the drawback is that deracemization by abrasive grinding cannot easily be upscaled, as high energy input is required, resulting in a more expensive equipment [20]. Even if ultrasound is used [21, 22], it has to be dealt with the non-homogeneity of the ultrasonic field [23].

Therefore, the idea of using temperature cycling was developed. The deracemization takes place due to similar effects, but no attrition is needed. The energy is provided to the system by temperature cycles [8]. However, high energy quantities are needed for heating and cooling a large amount of suspension, as well as a sufficient heat transfer area. Thus, it was also successfully tried not to force one single tank to a temperature program, but to circulate the suspension between two tanks with different temperatures [24]. Even though this is a promising method, upscaling might still be challenging as it might be difficult to obtain the exact same conditions spatially in both tanks.

All processes described yet are performed in batch mode. This is one of three process modes, which are used to classify crystallization devices. The other two are semi-batch and continuous [25]. Nowadays, most crystallization processes in the pharmaceutical industry are batch or semi-batch [10], but continuous crystallizers are more demanded recently [26], due to several advantages. Some of this are that a faster heat transfer is possible compared

to batch reactors [9, 10, 11], the setup is more simple [12] and often smaller. This results in lower costs [27] and the safety and economy of the process are often better. Also, the scale up is easier and some results can simply not be achieved via batch crystallization [26].

Therefore, in this master's thesis, we wanted to investigate if deracemization by temperature cycles can be performed in continuous flow. This would make upscaling easier, since only several crystallizers have to be installed in parallel, preventing spatial non-homogeneities of the temperature [10]. Moreover, the process would have also other benefits from being done in a tubular reactor, most important are the fast heat transfer and the simple setup. Thus, it is also investigated if enantiomeric purity can be achieved faster than in batch experiments.

For proof of concept, crystals in their respective saturated solution were cycled through a tubular reactor that was immersed in two water baths. The enantiomeric purity of the product was analyzed by Polarimetry or chiral HPLC, which is the most accurate measurement for determination of the enantiomeric excess yet [28]. Since deracemization is a stoichastic process [29], it was also beneficial to add enantiomerically enriched crystals to force the system in one direction. Furthermore, two possibilities to increase the residence time were investigated. The first was to use a recycle loop and pump the suspension several times through the tube and the second to use low pump rates and build up a slug flow profile with air to hinder crystals from sedimentation. A slug flow had also the advantage that it was not likely for crystals to change the fluid compartment, in which they were moving, often. Therefore, all crystals were for a similar time in the tube, which resulted in a narrow residence time distribution [12].

Last but not least, the influence of the water bath temperature difference, catalyst amount, pump rate and crystal mass were investigated to determine their influence on the deracemization progress per cycle. Also the effect on the total process was examined, to determine the optimal process conditions and the shortest process time.

2 Theoretical background

2.1 Crystallization

Crystallization is a process, when solids with a long-range molecular order (crystals) form from a melt or solution. The ordered molecules build up a crystal lattice, which is characteristic for the substance and also responsible for the outer appearance of crystals, meaning flat faces and well-defined angles [30].

One important property of a substance is the solubility or saturation concentration. It is defined as maximum solid amount of a substance which can be dissolved in a solvent at given pressure and temperature. Normally, the pressure dependence can be neglected, but the temperature dependence is important for a crystallization process. Therefore, the correlation of the saturation concentration and the temperature is often represented graphically, which is called solubility curve. Such a curve can be seen in figure 2.1. Also, the solvent and other components influence the system, so one curve represents only one particular solvent or solvent mixture, usually without any other dissolved substances present [31].

The solubility curve (individual points are also called clear points), separates the undersaturated area from the metastable zone. In this zone, the solution is supersaturated, but no spontaneous nucleation occurs in a certain finite time. Spontaneous nucleation, meaning the generation of new crystals, can occur either as primary or secondary nucleation. The latter is induced by solute particles and the former by other solid substances (heterogeneous) or can occur in the absence of any other solid substances (homogeneous). However, crystal growth is possible in the metastable zone. Seeds are added in this region in industrial applications, to grow, avoid nucleation and make the process more robust. Care has to be taken that the process conditions are not too close to the second line limiting the metastable zone, since this indicates when spontaneous nucleation occurs (individual points are also called cloud points) and is a kinetic value. It is shown in figure 2.1 as dashed line and depends mostly on the rate the system reaches supersaturation, e.g. the cooling rate for cooling crystallization [31, 32, 33].

For the measurement of the solubility curves, isothermal or polythermal methods are used. Isothermal methods are performed at constant temperature, either via the addition of solid until the solvent is saturated (addition method), or the equilibration of a solution with solid in excess and analysis after phase separation (excess method). In contrast to this, the suspension temperature is changed for polythermal methods, as a solution containing a defined amount of solid in excess is heated until all crystals are dissolved. The detection of the clear

points can be performed for example visually with a Crystalline® device, see chapter 3.4.1. In the reverse process, also the cloud points and therefore the width of the metastable zone can be detected [31].

In figure 2.1, also the process routes for two common crystallization processes are shown: cooling and evaporation crystallization. During cooling crystallization, the temperature of the suspension is lowered until supersaturation is reached, whereby the concentration of the solid in the solvent does not change. Contrary, evaporation crystallization is performed at constant temperature but changing concentration, as the solvent is evaporated. Also, crystallizations can be performed via the formation of a product (reactive crystallization) or lowering the solubility of the solvent, for example with an anti-solvent. However, the most commonly used process is the cooling crystallization [34]. It may also be mentioned that altough for a crystallization it is not necessary that a reaction takes place, it is common to refer to a crystallizer as a crystallization reactor [35].

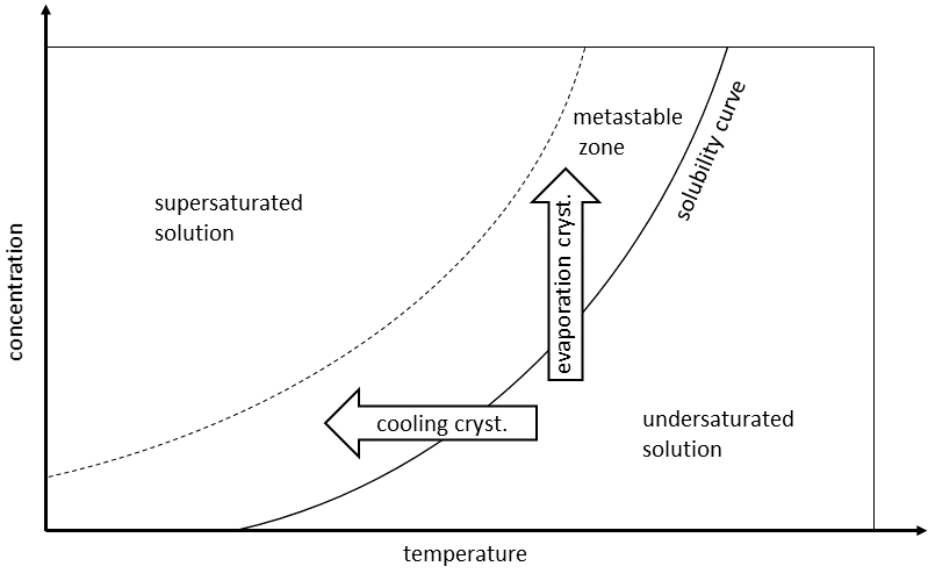

Figure 2.1: Solubility curve, adopted from [34].

2.2 Stereochemistry

Isomers are molecules with the same molecular formula but different molecular structures. They can be further specified as constitution isomers, including molecules, which have a different connection of the atoms, or configuration isomers, also called stereoisomers, only differing in the arrangement of the atoms in space [36].

If stereoisomers are related like image and mirror image, they are chiral and called enantiomers. The chemical and physical properties of two enantiomers are identical as well as

the reactions they undergo in an achiral environment. However, they behave differently in a chiral environment, like in many living cells. The only physical property which is different is the optical activity, meaning the ability to rotate plane-polarized light [13].

If two enantiomers form an equimolar mixture, it is optically inactive and called racemat. If the mixture is not equimolar, the enantiomeric excess *ee* is used to quantify the enantiomeric purity. It is defined as

$$ee\,[\%] = \frac{|R - S|}{R + S} \cdot 100\,\% \tag{2.1}$$

with the amounts of the enantiomers R and S [36]. R stands for rectus (right) and S for sinister (left). These names for the enantiomers result from the R, S or Cahn-Ignold-Prelog system for nomenclature [13]. The system can be applied to each stereogenic unit of a molecule, for example a stereocenter. Often, a carbon atom is the stereocenter, but it could be also another tetravalent and tetrahedrally coordinated atom [36]. For the nomenclature of a carbon, the four different groups bound are ranked from highest to lowest priority. Then, the molecule is rotated in a way that the lowest priority group points away from the observer. In a next step, the remaining groups are connected as ranked. If this connection is clockwise, the molecule is R, otherwise it is S [13].

In nature a wide-ranging chiral asymmetry is present. Many biologically significant molecules are homochiral, like L-amino acids and D-sugars [37]. Yet it is assumed, that this homochirality can be explained by the deracemization process due to temperature cycles [8], see chapter 2.4.2 for the mechanisms. Cycles near ambient temperature are omnipresent and can occur due to several reasons. For example, they can result due to diurnal and annual temperature changes, but also buoyancy or natural convection can induce a flow. It is also assumed, that not even a racemization agent is necessary in the liquid phase, since amino acids can racemize naturally in large time intervals [8].

However, if the theory is considered that underwater volcanic vents are the original source of life, for a review see [38], this could be also the reason for homochirality in nature. Between the vents and the surrounding deep water strong temperature gradients are present, which induce buoyancy flows. Moreover, it is likely that there are precursor compounds of amino acids present [8].

2.3 Analysis of chiral compounds

Chiral analysis deals with the measurement of two important quantities of chiral molecules: the absolute configuration and the enantiomeric excess. The following text provides an overview of some classical analytical methods [28]:

First, the absolute configuration of molecules can be determined by spectroscopic methods. Chiroptical spectroscopy methods are optical rotatory dispersion, which is also called polarimetry, circular dichroism and vibrational Raman optical activity. The analysis via

polarimetry relies on the fact that chiral compounds rotate polarized light [39]. The measurement principle can be seen in figure 2.2. Monochromatic light is polarized and passes the sample tube with the dissolved sample. Afterwards, it passes a second polarization filter for analysis. This filter rotates to match the plane of the polarized light, so that the light can pass the filter with maximal intensity. The angle of the analyzer corresponds to the optical rotation [13], which direction and magnitude is specific for each substance. However, it is also dependent on the wavelength of the polarized light, the temperature, the solvent, the concentration of the analyzed sample and the length of the light path through the sample in the sample tube. Therefore, to compare different samples, the specific rotation is used, which is defined as

$$[\alpha] = \frac{\alpha}{c \cdot l} \tag{2.2}$$

with the rotation α in degree, the concentration c in g/cm^3 and the path length l in dm [39]. Since enantiomers rotate monochromatic light with the same magnitude in opposite directions, the configuration of a sample only containing one enantiomer can be determined by the sign of the angle. Further, the enantiomeric excess of samples containing both enantiomers can be determined, as a racemate is optically inactive. The *ee* corresponds to the optical purity, which is defined as ratio of the observed specific rotation of the sample $[\alpha]$ to the specific rotation of the pure enantiomer $[\alpha]_0$

$$\text{optical purity}\,[\%] = \frac{[\alpha] \cdot 100\,\%}{[\alpha]_0}. \tag{2.3}$$

Care has to be taken that no optically active impurities are present [36].

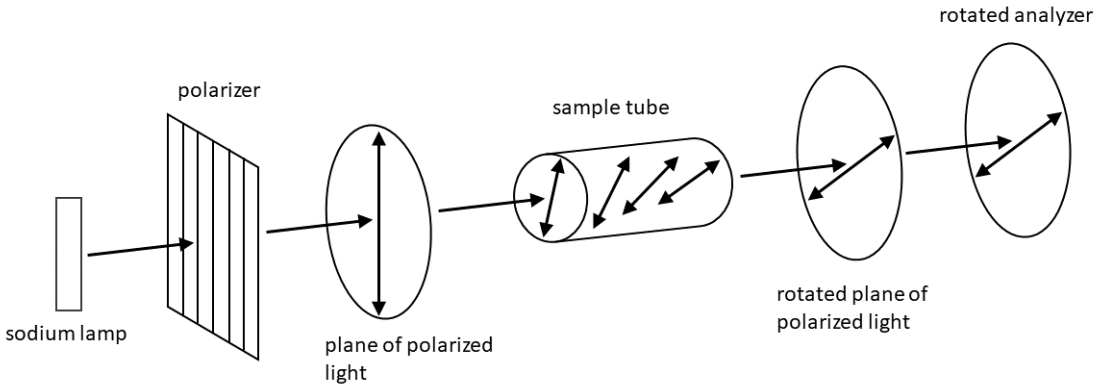

Figure 2.2: Scheme of a polarimeter, adopted from [13].

The measurement via electronic or vibrational circular dichroism, however, takes into account that the difference of absorbance of left and right polarized light is related to the concentration of chiral molecules. And vibrational Raman optical activity relies on differential Raman scattering of molecules excited with left and right circularly polarized laser light or the change of intensity of such left and right circularly polarized light components, when using linear/unpolarized laser light [39].

A second possibility to determine chiral substances is via separation of the enantiomers. Therefore, chiral selectors are used, which build temporary diastereomeric complexes with the substance. Depending whether chromatographic or capillary electromigration techniques are used, the selectors can be in the mobile phase, fixed to a solid or in the background electrolyte. The most relevant chromatographic techniques include gas, high-performance liquid (HPLC), super- and subcritical fluid chromatography and capillary electromigration techniques include diverse kinds of electrokinetic chromatrography, capillary electrochromatrography and capillary electrophoresis [14].

For the determination of the enantiomeric excess, HPLC is the standard method today, since high sensitivities of 0.1 % can be achieved. However, also vibrational circular dichroism or Raman optical activity are used, although they can only achieve sensitivities of 1 %. This techniques have the advantages that no separation of the enantiomers is necessary, the substance to be analyzed does not have to be dissolved, making measurements in various states of environment possible, and that real time in situ measurements can be performed. Also the combination of this two techniques, vibrational optical activity, is used [28].

Further techniques to be mentioned are X-ray crystallography and nuclear magnetic resonance (NMR). X-ray crystallography is a reliable method for the determination of the absolute configuration of a molecule [40] and by NMR, the absolute configuration as well as the enantiomeric purity can be detected. Therefore, the classical NMR has to be adopted for measurements of chiral molecules. Either chiral derivatizing agents, chiral solvating agents or chiral lanthanide shift reagents are used to form diastereomers, which resonances can then be detected. The diastereomer formation takes place with the derivatizing agents by covalent bindings and chiral solvating agents by hydrogen bonds, dipole–dipole, or $\pi - \pi$ interactions. The lanthanide shift reagents are similar to the chiral solvating agents with the difference that the lanthanide shift reagents include a paramagnetic center [41].

2.4 Chiral resolution

The separation of the enantiomers is called resolution [36]. Some methods for this procedure were already discussed in chapter 2.3, as they are also used for the analysis of chiral molecules. These rely on the formation of diastereomers [19]. Other methods are for example preferential crystallization [16], or the use of substrate selective reactions [17]. For the latter, also often enantioselective catalysts or enzymes are used [18].

However, only a yield of 50 % could be achieved without an additional unit to convert one of the enantiomers into the other [5]. Thus, Havinga et al. combined crystallization with a racemization reaction in solution. If enantiopure seeds are introduced in a supersaturated solution, they grow until depletion of the racemate from the solution is achieved. This process is called total spontaneous resolution [42].

Yet, Viedma ripening and the temperature cycling method are especially promising, since deracemization can occur even with a racemic solid state. This results in a complete conversion of the unwanted to the desired enantiomer [6, 43]. The process is described in detail in the following.

2.4.1 Attrition enhanced (Viedma) ripening

A process, in which total resolution is achieved during isothermal wet milling is called Viedma ripening. It is named after Viedma, who first discovered that under such conditions the intrinsically achiral $NaClO_3$ deracemizes [6]. Later, it was shown that this also works for intrinsically chiral substances, whereby even in solution both enantiomers are present, when they can undergo a racemization reaction. The difference between intrinsically achiral and chiral substances is pointed out in figure 2.3 [7].

On the left side, an intrinsically achiral substance is shown. The black rectangular at the top indicates that in solution only one form exists. This substance can crystallize via the black arrows to one of the two solid phase identities, indicated as blue and green mirror related diamonds. Both solid identities are marked as A, as both can dissolve to form again the rectangular without chiral identity, resulting in an equilibrium reaction. Therefore, the dissolution is also indicated via two arrows [7].

Contrary to this, even in solution both chiral identities of an intrinsically chiral substance are present, as illustrated on the right side of the figure. The molecules are always either of the R or S form, which is again indicated via the blue and green mirror related diamonds. Moreover, they can also undergo crystallization and dissolution processes via the four arrows, whereby the S form can not crystallize to the R form and vice versa. A change of the chiral identity is only possible via a racemization reaction in solution, which is also an equilibrium reaction and indicated via two more arrows [7].

However, the intrinsically achiral and chiral substances have in common that in the solid phase only crystals with separate identity are formed [7]. Systems of such pure enantiomeric crystals are called conglomerates [44], but unfortunately, only about 10 % of the known chiral molecules crystallize as such [45]. Yet it was recently shown that some compounds are still suitable for Viedma ripening as they form conglomerate salts [46, 47].

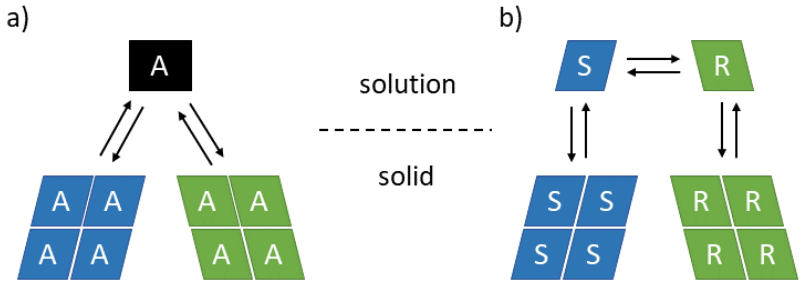

Figure 2.3: Difference between an intrinsically achiral molecule (a) and an intrinsically chiral molecule (b) undergoing racemization in solution, adopted from [7].

For Viedma ripening a saturated solution with additional solid crystals and the catalyst is stirred in a flask. In a first attempt, attrition was induced via glass beads [6], but later also ultrasound was used [21, 22].

During the process, two main mechanisms occur [48, 49, 50]:

1. Ostwald ripening
2. Enantioselective agglomeration of particles of different size.

The agglomeration of crystals results in bigger enantiopure crystals, which can not dissolve, leading to an asymmetry in the system. Ostwald ripening promotes this, since the smallest particles dissolve in a saturated solution for the growth of bigger ones.

The effect is enhanced while grinding since the solubility of the crystals depends on their size due to Gibbs-Thomson rule [51]. Moreover, the surface area is increasing, which is a driving force for crystal growth, whereby the relative increase of the surface area of the desired enantiomer is higher. Therefore, the asymmetry in the solid phase in combination with the racemization reaction in the solution results in the deracemization of the crystals [7].

In figure 2.4, the process favoring the S enantiomer is illustrated in a phase diagram, whereby the orange shaded area indicates the region, which is not accessible for the system. The composition of the mother liquid is constant during the whole process, which is indicated by the blue dot. However, the concentration of the solid evolves towards the S enantiomer (green arrows) and the overall excess (red arrows) towards the limit of the orange area, meaning the biphasic domain [52].

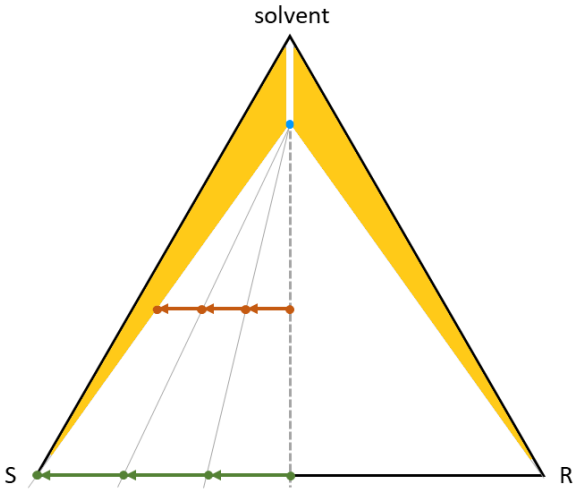

Figure 2.4: Illustration of Viedma ripening favoring the S enantiomer in a phase diagram, blue dot corresponds to liquid composition, green dots to solid composition and red dots to overall composition, adopted from [52].

The outcome of the deracemization of an exact racemic system should be stochastic, since both enantiomers have identical thermodynamic properties. Therefore, the induced spatial asymmetry that leads to the deracemization, which is also called symmetry breaking, should occur due to random fluctuations. Contrary, in practice a preference is observed, whereas chiral impurities are considered to be the main reason for that [29]. This preference could be overcome for example via applying ultrasonic waves [53] or high attrition intensities [29].

However, it can be also desired to favor one enantiomer and there are several possibilities for this [29]. For example, the process could be started with an initial enantiomeric excess, or chiral additives could be used [7]. In the latter case, the enantiomer with the chirality opposite to the added chiral species is favored due to Lahav's rule of reversal [54, 55]. Another possibility would be the use of crystals of different size. The initially larger particles can determine the chiral end state, even if the smaller are present in enantiomeric excess [56, 53]. Finally, it is also possible to influence the chiral end state with circularly polarized light [57].

2.4.2 Deracemization via temperature cycles

First, it was discovered with a boiling suspension of sodium chlorate that deracemization could be also achieved in the absence of grinding due to a temperature gradient. It was suggested, that the crystals undergo cycles of dissolution and crystallization while moving between the hot plate and the surface of the suspension [58]. Later, programmed heating-cooling cycles were used [43]. Like attrition enhanced cycling, this can either be performed with conglomerate forming compounds [45] or compounds that form conglomerate salts [20].

For the process, no attrition is necessary, as the energy is induced in the system via the heating-cooling cycles. One cycle consists of an isothermal period at low temperature at the beginning, a linear increase to a higher temperature, an isothermal period at the higher temperature and finally a linear decrease to the starting temperature. These cycles are repeated several times, as done by Suwannasang et al. [8]. They also tried to optimize it via varying the cycles during the process, like damping the cycles. Therefore, the maximum temperature of each cycle was lower than the maximum temperature of the previous one and the minimum temperature higher than the last minimum temperature. However, they only performed batch experiments [43].

The mechanisms leading to deracemization in systems with temperature fluctuations are similar to the mechanisms occuring during Viedma ripening. The asymmetry in the solid phase increases also due to enantioselective agglomeration and dissolution of small crystals [59]. It is even suspected that the effects during grinding are due to the fact that attrition induces local high temperatures and are therefore similar [8]. However, the deracemization via temperature cycling proceeds generally with a higher rate, due to reasons that are not understood yet [8, 60].

The deracemization process for a system forced to temperature cycles can be seen in figure 2.5 for a system enriched in S [61]. The mechanisms were discussed by Suwannasang et al. and Breveglieri et al. [8, 61]. During the heating period, the crystals are partially dissolved, yielding a racemic mixture, as long as the *ee* of the solid phase is not too high. If it is, more of the S enantiomer will dissolve but nevertheless the excess of R in the solid phase is enriched, as proportionally more of the R enantiomer is dissolved. During the cooling period, recrystallization of the same amount of mass, which was dissolved, takes place. Since more surface of the S enantiomer is available, this crystals will grow faster and agglomerate more (entrainment effect). This induces an *ee* in the saturated solution, which is then compensated by a racemization reaction. Therefore, after each cycle, the S enantiomer in the solid phase is more enriched. Breakage of the crystals can occur, but for this system it is not crucial.

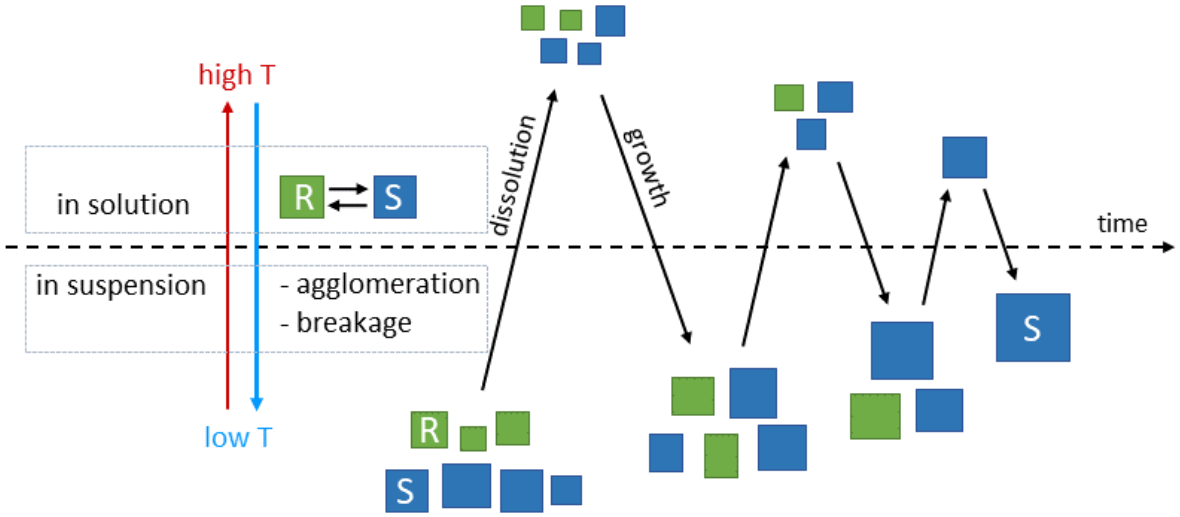

Figure 2.5: Time dependent deracemization via temperature cycles, adopted from [61].

It has been observed that the deracemization reaction is autocatalytic and the *ee* over time gives a sigmoidal curve with an exponential part, whereby it is assumed that at optimal process conditions it is fully exponential for conglomerates without partial solid solution [8, 62]. The exponential increase can be written as

$$ee = ee_0 \cdot e^{k \cdot t} \tag{2.4}$$

with the enantiomeric excess at the beginning ee_0, the deracemization constant k and the time t [63]. As result, with increasing initial enantiomeric excess, the deracemization is accelerated and also the experimental reproducibility is improved [20, 22, 64]. However, this was observed at isothermal conditions. During temperature cycles, the constant k likely varies with varying temperatures [59], giving an average value over the whole experiment. Furthermore, it is not possible to compare deracemization processes with a different total time. To make this comparable, the enantiomeric excess can also be related with the cycle number based deracemization constant k_N to the number of temperature cycles N [20]

$$ee = ee_0 \cdot e^{k_N \cdot N}. \tag{2.5}$$

Therefore, the system is sensitive to the initial enantiomeric excess. Other parameters that influence the system are the temperature difference, amount of catalyst, residence time and amount of solid crystals, which will be discussed in chapter 4.3. Whether the cooling rate influences the total process time, is still not clarified. On the one hand, it was observed by Suwannasang et al. that an increase of the cooling rate does not affect the total process time, as secondary nucleation of the minor enantiomer occurs. So each cycle is shorter, but more cycles are needed to achieve total resolution [8]. On the other hand, Breveglieri et

al. [61], detected for *N*-(2-methylbenzylidene)-phenylglycine amide that even with a higher number of cycles, the total time can decrease if each cycle is shorter but there is an asymptotic behavior for infinitely high cooling rates. And Cameli et al. [65], who observed similar results as Breveglieri, even suggests that secondary nucleation might contribute to enabling deracemization via temperature cycling for certain compounds. Secondary nucleation can cause enantiomeric enrichment due to autocatalysis and mutual inhibition, which is the competition of the growing nuclei of both enantiomers for the same supersaturation, due to fast racemization in solution [65, 66]. Similarly, they also expect an influence of a fast heating rate. Since in a tubular reactor the cooling and heating rates are fast, as already mentioned in chapter 2.5, the heat transfer rates should either shorten the overall process time or do not affect the process at all.

Further, different models were established to describe the process. Katsuno et al. [59] supposed that the process is accelerated by small clusters and not by monomers, as the mass flow of small clusters is more effective. At the cooling period, the small clusters of the enantiomer in excess are nearly twice as fast incorporated into solids as small clusters of the other enantiomer, which dissociate into monomers due to the large effective surface tension. Then, this excess of monomers of the minority species is transformed via the racemization reaction to monomers of the majority species, which therefore build small clusters during heating. A second model investigated by Uchin et al. and Suwannasang et al. uses the crystal growth rate dispersion [67, 68].

Last but not least, it has to be mentioned that the deracemization process was improved via cycling the suspension between a colder and a warmer vessel by Suwannasang et al., making a temperature control system capable of heating and cooling redundant. The process was performed with two round bottom flasks with double jackets which were connected to temperature controlled baths. To ensure inside uniform temperature, the suspension was stirred. Finally, the transportation between the flasks was achieved with the use of a peristaltic pump [24].

2.5 Tubular reactors

In a tubular reactor, the reaction mixture flows through a cylindrical pipe, while the reactants are consumed. This results in a varying composition in axial direction. For simplification and description, it is common to assume a plug flow profile meaning that concentration, reaction rate, velocity and temperature are radially uniform [69]. In figure 2.6 a plug flow reactor is schematically shown and in figure 2.7 the concentration profile for a constant density reaction, whereby c_{A0} is the concentration of the substance A entering the reactor, c_A the concentration of the same substance leaving the reactor and Z_1, Z_2 and Z_3 the locations of three cross sections through the reactor. One can see that the concentration of A entering the reactor decreases via the reactor length as it is consumed. However, it does not change temporal at any cross section of the reactor.

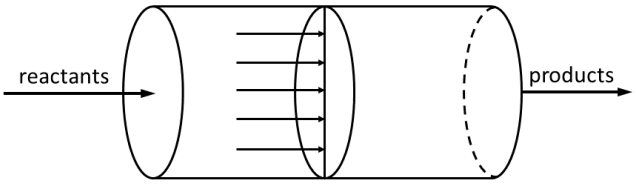

Figure 2.6: Scheme of a tubular reactor, adopted from [69].

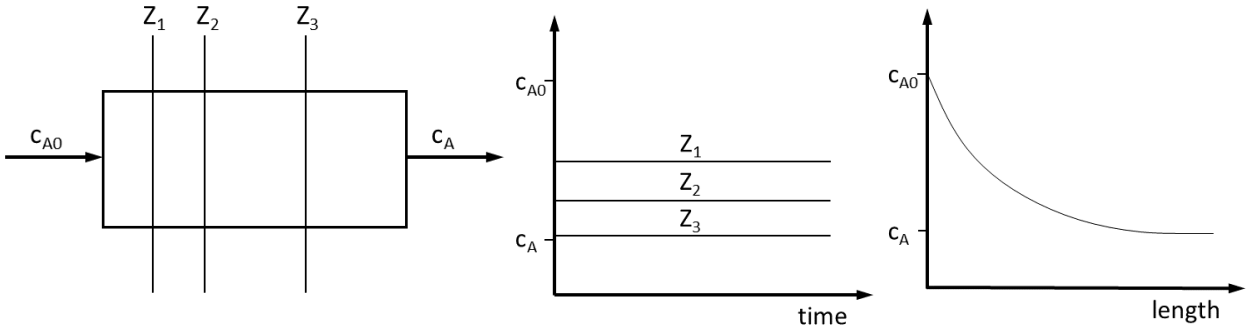

Figure 2.7: Temporary and local dependence of the concentration of a substance in a tubular reactor for a constant density system, adopted from [70].

The necessary total volume for a given reaction can be derived from the material balance [71]

$$\text{input} = \text{output} + \text{disapperance by reaction} + \text{accumulation}. \tag{2.6}$$

Since the composition of the mixture changes along the length of the reactor, it has to be made for a differential volume element dV. Considering that no accumulation takes place, for a compound A it gives

$$F_A = F_A + dF_A + (-r_A) \cdot dV \tag{2.7}$$

with the input F_A, the output $F_A + dF_A$ and the reaction rate $-r_A$. Inserting the conversion $X_A = \frac{F_{A0} - F_A}{F_{A0}}$

$$dF_A = -F_{A0} \cdot dX_A \tag{2.8}$$

and integration finally gives the total reactor volume

$$V = F_{A0} \cdot \int_0^{X_A} \frac{dX'_A}{-r_A}. \tag{2.9}$$

Moreover, the energy balance for a tubular reactor in steady state can be written as [72]

$$\dot{Q} - \dot{W}_s - F_{A0} \cdot \sum_{i=1}^{n} \Theta_i \cdot cp_i \cdot (T - T_{i0}) - \Delta H_R(T) \cdot F_{A0} \cdot X_A = 0, \tag{2.10}$$

with the heat added to the reactor $\dot{Q}$, the shaft term $\dot{W}_s$, the entering molar flow of the limiting reacting component F_{A0}, the ratio of number of moles entering of species i and A Θ_i, the specific heat capacity of the species i cp_i, the temperature of the leaving flow T, the temperature of each species i when entering the reactor T_{i0}, which is often for each species i the same and referred to as T_0, the heat of reaction at the temperature T per mole A $\Delta H_R(T)$ and the conversion of the limiting substance X_A. The shaft term corresponds to work, which is added to the system, for example the work which is produced by a turbine in a tubular reactor. Often it can be neglected.

The heat of reaction can be expressed with the heat of reaction at a reference temperature $\Delta H_R^\circ(T_R)$ and the change of the heat capacity per mole of the limiting substance reacted Δcp

$$\Delta H_R(T) = \Delta H_R^\circ(T_R) + \Delta cp \cdot (T - T_R). \tag{2.11}$$

With this, the conversion of adiabatic processes, meaning that no heat is exchanged with the environment, resulting in $\dot{Q} = 0$, can be expressed via the energy balance (2.10)

$$X_A = \frac{\sum_{i=1}^{n} \Theta_i \cdot cp_i \cdot (T - T_0)}{-(\Delta H_R^\circ(T_R) + \Delta cp \cdot (T - T_R))}. \tag{2.12}$$

Rearrangement gives the outlet temperature of a tubular reactor

$$T = \frac{X_A \cdot (-\Delta H_R^\circ(T_R)) + \sum_{i=1}^{n} \Theta_i \cdot cp_i \cdot T_0 + X_A \cdot \Delta cp \cdot T_R}{\sum_{i=1}^{n} \Theta_i \cdot cp_i + X_A \cdot \Delta cp}. \tag{2.13}$$

Reactors for continuous crystallization can operate with a throughput in a range of several liters per hour in residence times of a few minutes [12]. They are typically characterised by a length >1 m and an inner diameter <10 cm. This high surface to volume ratio enables a faster heat transfer compared to batch reactors, which makes a fast switch between super- and undersaturation possible [9, 10, 11]. Another benefit is that the setup is simple and the crystal breakage is reduced due to the absence of moving parts [12]. Finally, a traditional scale up could be avoided, as reactors can be installed parallel [10].

However, tubular reactors can be plugged if fouling occurs. This is tried to be overcome by operating with segmented or slug flow, via adding gas or any other immiscible fluid. As all compartments need the same time through the reactor and there is less backmixing, this has also the benefit that the residence time distribution is smaller as without slug flow [73]. Another issue, which has to be overcome, is that the total length of the reactor is limited and therefore the residence time, since the pressure drop of the reactor has to be lower than the maximum pressure of the pump [12]. Moreover, the flow rates could also not be too low to avoid plugging [10].

3 Experimental part

3.1 Model system

As model substance, the intrinsically chiral *N*-(2-methylbenzylidene)-phenylglycine amide, short NMPA, was used. It racemizes in solution with the base 1,8-diazabicyclo[5.4.0]undec-7-ene, short DBU, as catalyst, the structures can be taken from figures 3.1 and 3.2. One advantage of the use of an intrinsically chiral substance in contrast to an intrinsically achiral substance is that more tools can be used for the analysis of the *ee*. As discussed in chapter 2.3, methods like polarimetry or HPLC can measure only dissolved compounds and since intrinsically achiral substances have no chiral identity when in solution, see chapter 2.4.1, the determination of the enantiomeric excess with such devices is not possible.

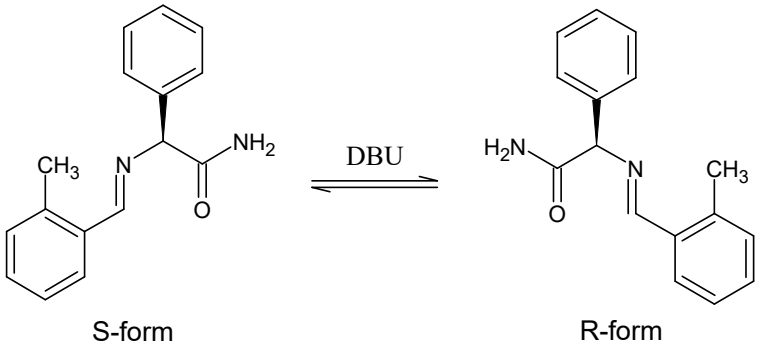

Figure 3.1: Racemization reaction of NMPA in solution [61].

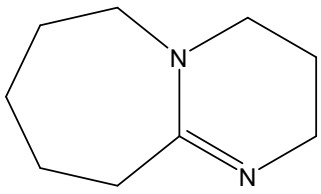

Figure 3.2: Structure of DBU [61].

3.2 Crystal analysis

The measurement of the enantiomeric purity was performed by HPLC with the chiral column Chiralcel OJ-H, 250 mm x 4.6 mm, particle size 5 µm, at a pressure of 47 bar and a temperature of 25 °C. The eluent was a mixture of n-hexane and isopropanol in the volumetric ratio

80:20, the injection volume was 1 µL. About 5.5 mg of the samples were dissolved in 8 mL of a volumetric 50:50 mixture of n-hexane and isopropanol. The maximum sample amount of 5.7 mg was never exceeded to avoid particles precipitating by contact with the eluent, since the solubility in n-hexane is limited. The analysis was carried out at 210 nm for the detection of the side products, as it is likely that the diastereomer 2-(2-methylphenyl)-5-phenyl-imidazolidin-4-one forms [7], and at 254 nm, as it is more accurate for NMPA. The retention time were 11.4 min and 17.4 min, whereby the first was for the S-form and the second for the R-form [7]. The enantiomeric excess was calculated from the peak areas.

For estimations of the crystal size, the microscope DM4000 M from Leica was used and for the determination of the particle size distribution the device HELOS® H2395 from Sympathec via laser diffraction, whereby the particles had to be in suspension. Therefore, the solvent was stirred for 2 h with an excess of NMPA, filtered and filled in a cuvette. Then, the crystals were added. As solvent either water or ethanol was used, since the solubility of NMPA in water is lower, but ethanol is used during the experiments. At the measurements with water also a droplet of Tween 80 had to be added to reduce the surface tension.

Finally, the solubility measurements were performed visually with a Crystalline® device from Technobis.

3.3 Preparation of NMPA

The crystals were synthesized as described in literature [7] and the purity confirmed by chiral HPLC. The used chemicals were purchased from the providers as listed in the appendix 7.1 and used as received. To ensure small and uniform particle sizes, the crystals were ground with mortar and pestle. The crystals were analyzed from time to time using a microscope, whereby at the beginning some crystals were approximately twice or three times as big as the smallest. The grinding was considered sufficient when no crystals larger than 30 µm could be detected. Pictures of the crystals before grinding and afterwards can be seen in figure 3.3.

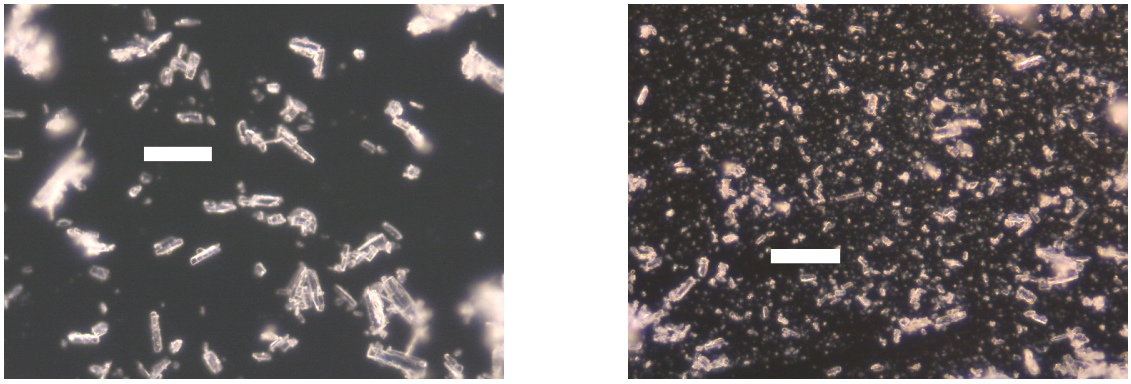

Figure 3.3: Microscopic picture of NMPA crystals, not ground (left picture) and ground (right picture), white bar indicates a length of 50 µm.

For the determination of the particle size distribution of the single crystals, the NMPA was analyzed with the device HELOS®. The particles were added to the saturated water resulting in a solid concentration of 8.33 %. It could be seen that immediately clusters formed, which were broken during the immersion of the cuvette of 1 s in an ultrasonic water bath. The cumulative and density distribution with the median of $x_{50} = 10.64\,\mu m$ can be taken from figure 3.4. It has to be mentioned that it is likely that small crystals dissolved during the measurement due to temperature fluctuations and the resulting change of the solubility of the crystals in water.

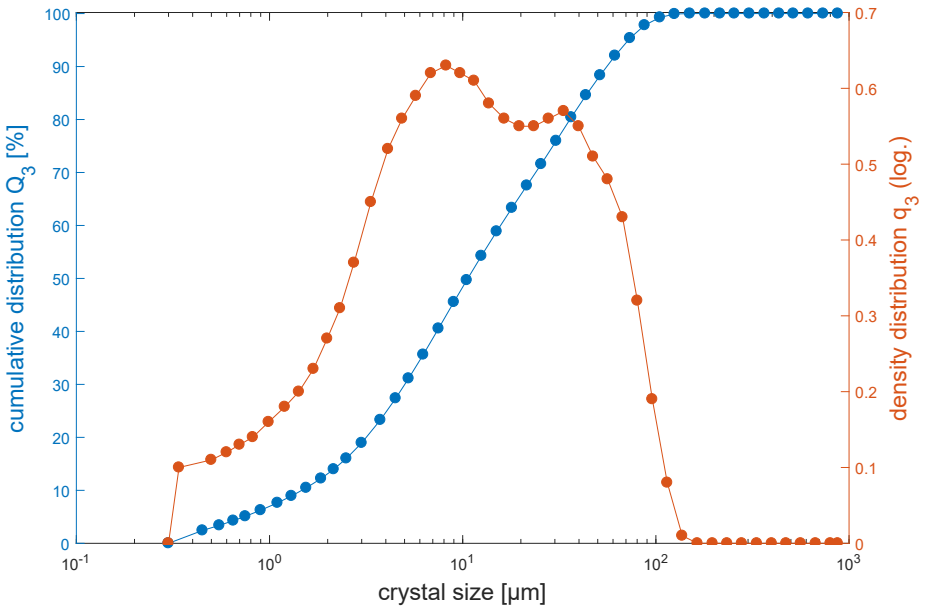

Figure 3.4: Cumulative and density distribution of NMPA crystals in water, after 1 s ultrasonic pulse, size of single crystals.

However, during the cycle experiments, it was likely that clusters formed. The results

from the measurement with the device HELOS® for a suspension in ethanol and a solid concentration of 19.43 %, which was not immersed in an ultrasonic bath, can be taken from figure 3.5. Due to the agglomerates, the measured particles were bigger than the single crystals, yielding a median of $x_{50} = 246.66\,\mu m$. For this measurement, the conditions might be closer to the conditions during the cycle experiments, but it is more inaccurate. The solubility of NMPA in ethanol is higher, as more NMPA has to be added to achieve saturation. Therefore, crystals dissolve more readily if temperature fluctuations occur and some precipitation could be detected with the bare eye as the cuvette was removed from the device after the measurement. Moreover, due to the size of the agglomerates, it is likely that some particles exceeded the measuring range of the HELOS® device.

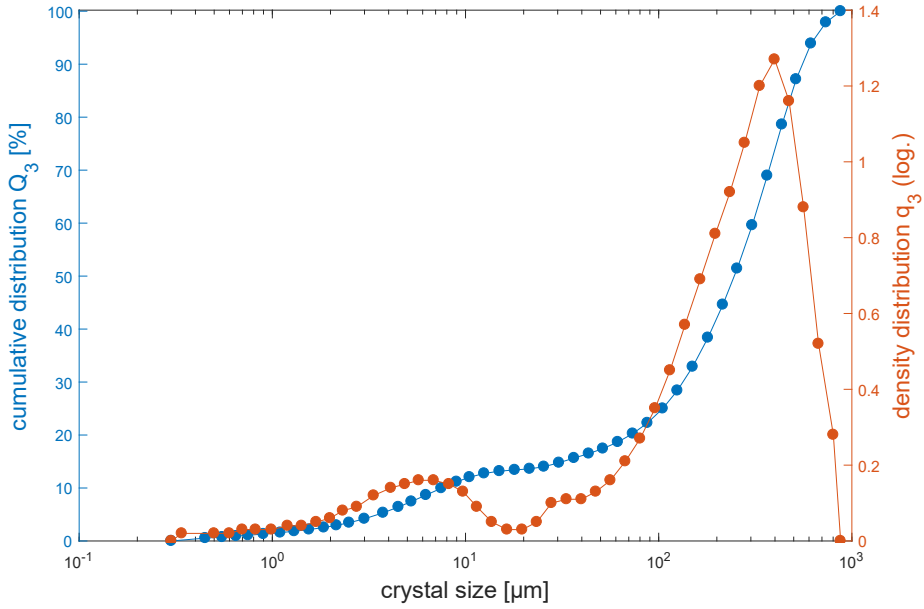

Figure 3.5: Cumulative and density distribution of NMPA crystals in ethanol, most likely size of agglomerates with which the experiments were performed.

For some experiments, to make an estimation of the influence of the particle size possible, the crystals were not ground but sieved. About 100 g NMPA were sieved with a sieving stack with the mesh sizes 200 µm and 50 µm. An amplitude of 1.44 mm/g was used and four soft rubber balls with a diameter of approximately 1.5 cm were added to break up clusters. The sieves were weighed every 10 min and the sieving stopped as soon as the change of the desired mass on the 50 µm sieve was less than 0.5 g, which was the case after 60 min.

3.3.1 Preparation of enantiomerically enriched NMPA

To achieve an enantiomeric enrichment of the crystals for establishing a desired starting enantiomeric excess, the Crystalline® device was used. This had the advantage that the vials could be forced to defined temperature cycles, which sped up the reaction as shown in

literature [61], but the drawback that the reaction volume was limited to 8 mL.

Approximately 0.16 g NMPA were used per vial. This consisted of about 0.12 g racemic NMPA and 0.04 g NMPA obtained from deracemization experiments in the tubular reactor to induce an enantioimbalance, which is necessary to ensure that the R-form is favored and also to speed up the reaction. However, since the *ee* of the NMPA from the experiments in the tubular reactor varied mostly between 10% and 20%, but also values as high as 60% were achieved, the ratio of racemic NMPA to NMPA from the experiments was varied to start all experiments in the Crystalline® device under roughly same conditions. Also approximately 6 g of ethanol saturated with NMPA in a round bottom flask at room temperature for 2 h was added to each vial together with 30 µL DBU. Therefore, 0.20 mmol DBU and about 0.64 mmol NMPA were present in each vial, see the appendix 7.2 for the substance properties.

The vials were exposed to temperature cycles according to literature [61] while stirring with 500 rpm with a 1 cm stirring bar. For the heating part, the temperature was increased from 22 °C to 35 °C with a heating rate of 1.3 °C/min, then held at this temperature for 10 min. For the cooling part, the vials were cooled with the same (negative) rate, -1.3 °C/min, and then again held for 10 min at 22 °C. This gave a total cycle time of 40 min, the temperature profile of one cycle is illustrated in figure 3.6.

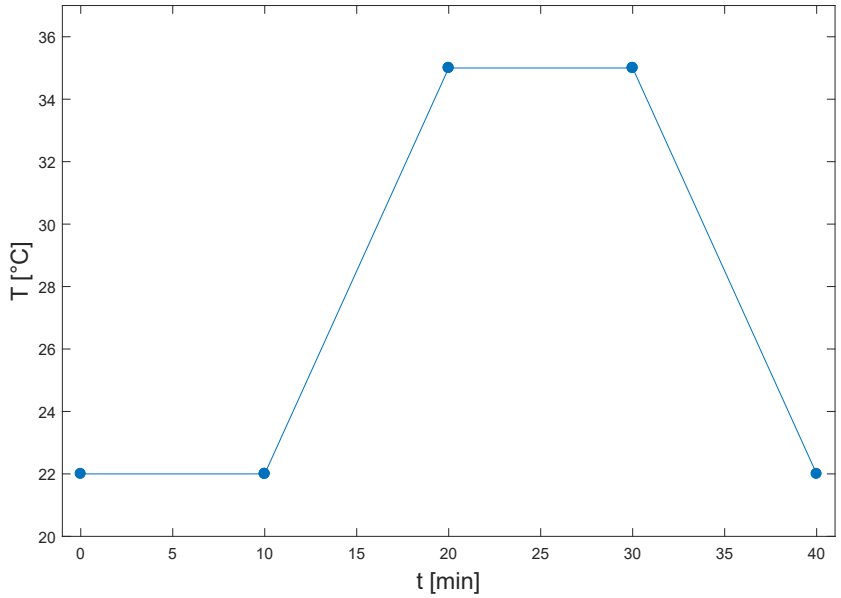

Figure 3.6: Profile of one temperature cycle for enantiomeric enrichment of NMPA in the Crystalline® device.

Mostly, the cycles had to be repeated for 9 days, which corresponded to approximately 320 cycles before the crystals were filtered and dried under vacuum. Typically, an enantiomeric excess of 50% to 60% was reached, which was confirmed by chiral HPLC and

considered sufficient for the experiments in the tubular reactor. Unfortunately, there was also a side product formation taking place. It is supposed, that the diastereomer 2-(2-methylphenyl)-5-phenyl-imidazolidin-4-one was formed [7], see figure 3.7. However, it is assumed that the side products just dissolve in ethanol during the deracemization experiments and do not influence the reaction. This is confirmed by the fact that no solid side products could be detected in the samples of the suspension prepared for the experiments in the tubular reactor.

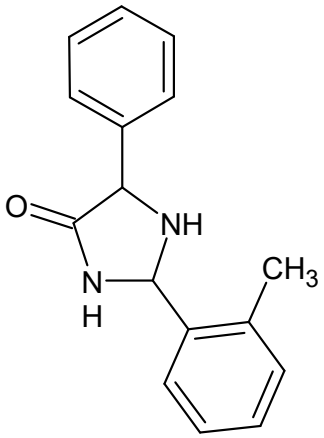

Figure 3.7: Structure of the side product 2-(2-methylphenyl)-5-phenyl-imidazolidin-4-one, obtained from ChemDraw®

Although at one experiment four vials had the same ee_0, the crystals of one vial had after a reaction time of 5 days an *ee* which was about 6 % higher than the *ee* of three other vials after 10 days. Since the filtration and drying of the sample of just one vial was faster, as the amount of crystals was smaller, it is an indication that during this processes a racemization reaction took place. However, for comparison of the experiments it is not necessary that all are performed with the same staring *ee*, as will be discussed in chapter 4.3.

Obviously, to ensure uniform particle sizes, it was also necessary to grind the enantiomerically enriched NMPA until the crystal size was comparable to the racemic crystals, which was confirmed via microscopy. However, to detect the influence of the particle size, also some crystals which were not ground were necessary for experiments. These were used directly after the temperature cycling, as sieving of such small amounts is not sufficient.

It may also be noted, that for the first enrichment, no NMPA from cycle experiments was available to favor one of the enantiomers. Therefore, the temperature cycling with the Crystalline® device was only performed with 0.2 g racemic NMPA, 5 g saturated ethanol and 19.26 µL DBU. This equates to 0.79 mmol NMPA and 0.13 mmol DBU. Since chiral HPLC showed that the product was enriched in the R-form, this was chosen as the desired enantiomer. Interestingly, this is the form, which was also preferred in literature during several experiments [29, 60].

3.4 Pre-experiments

3.4.1 Solubility of NMPA in ethanol

The temperature dependent solubility of NMPA in ethanol was determined with the Crystalline® device. Therefore, NMPA and ethanol were filled in vials to get concentrations between approximately 5.5 and 30.0 mg/g. The vials were shaken manually, until all crystals were dissolved. The solutions were stirred at 600 rpm with approximately 1 cm stirring bars and forced to defined temperature cycles in the Crystalline® device. It would have been sufficient to detect the dissolving temperatures, if the samples were only heated once, but for terms of reproducibility, the samples were heated with a rate of 0.5 °C/min to 70 °C and cooled with the same rate to -10 °C three times. The transmissivity was detected inline and a gradual increase corresponded to the clear point when all crystals were dissolved. However, at high temperatures a shift of the clear points to lower temperatures occurred, as obviously the NMPA is unstable at higher temperatures. Therefore, the experiment was repeated and the samples only heated to temperatures, which were a bit higher than the estimated dissolution temperatures of the first experiment, while stirred at 500 rpm. The exact values can be taken from the appendix 7.3.

The relation of the concentration of dissolved NMPA in ethanol and the temperature can be seen in figure 3.8, as well as the logarithmic regression of the data

$$c = 3.795 \cdot e^{0.047 \cdot T}, \tag{3.1}$$

were c is the concentration of NMPA in mg/g and T the temperature in °C. The regression gives a variance of $R^2 = 0.997$.

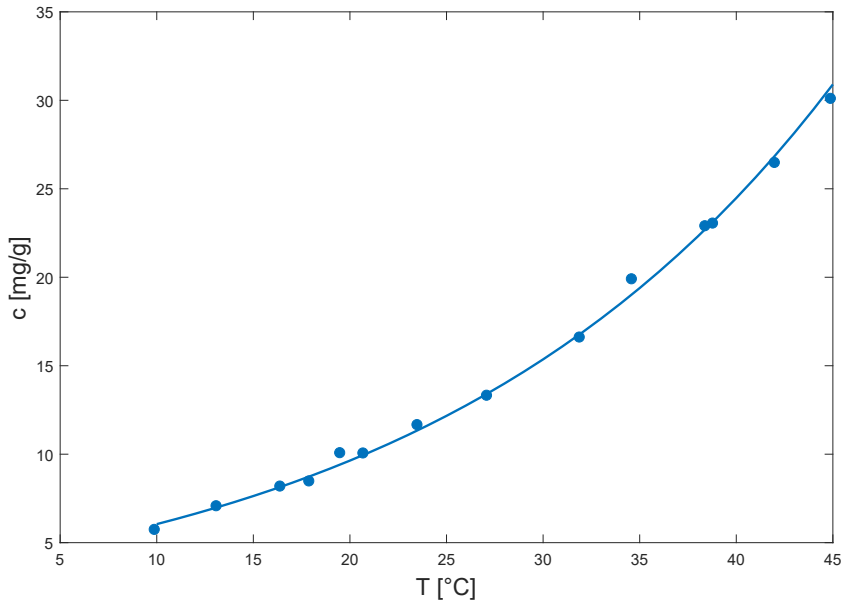

Figure 3.8: Solubility diagram of NMPA in ethanol, dots represent the clear point temperatures in °C for different concentrations of NMPA in mg/g, the curve is the solubility line fitted to the data, see equation (3.1).

This solubility curve can be also used to illustrate the process during temperature cycles, see figure 3.9 [61]. The deracemization experiments in the tubular reactor start with the conditions at point S, as the solution is saturated at ambient temperature, see chapter 3.6. Then, as the reactor immerses in the cold water bath, the operating line corresponds to the black arrow, and reaches via the blue arrow point A. During the heating period, when the temperature increases by ΔT, the operating line corresponds to the red arrow leading to point B. At higher temperature, the solubility of NMPA in ethanol increases, as can be seen by means of the solubility curve which is represented as solid, black line. As a result, the concentration of crystals Δc dissolves to reach point C and the equilibrium. Obviously, the operating line corresponding to the red arrows is only attended, if the heating is infinitely fast. Depending on the heating rate, the operating line can be anywhere in the red colored area. The slower it is, the more it corresponds to the solubility line. During the cooling period, a process analog to the heating takes place. If the cooling is infinitely fast, the temperature decreases by ΔT until the system reaches point D via the blue arrow, and crystallization takes place since the ethanol is supersaturated by Δc. The blue colored area hereby marks again every real conditions the system can reach. Since the heat transfer in a tubular reactor is fast, as discussed in chapter 2.5, it is assumed that the system corresponds rather to the arrows. However, this diagram illustrates the process provided that the system can reach the equilibrium. It has to be noted that Δc only corresponds to the maximum concentration change possible under this conditions. Depending on the actual kinetics, it is not given that at the maximum temperature the concentration of point C is reached, as it can also be lower. Respectively, the concentration at the lowest temperature can be higher

than that in point A [61].

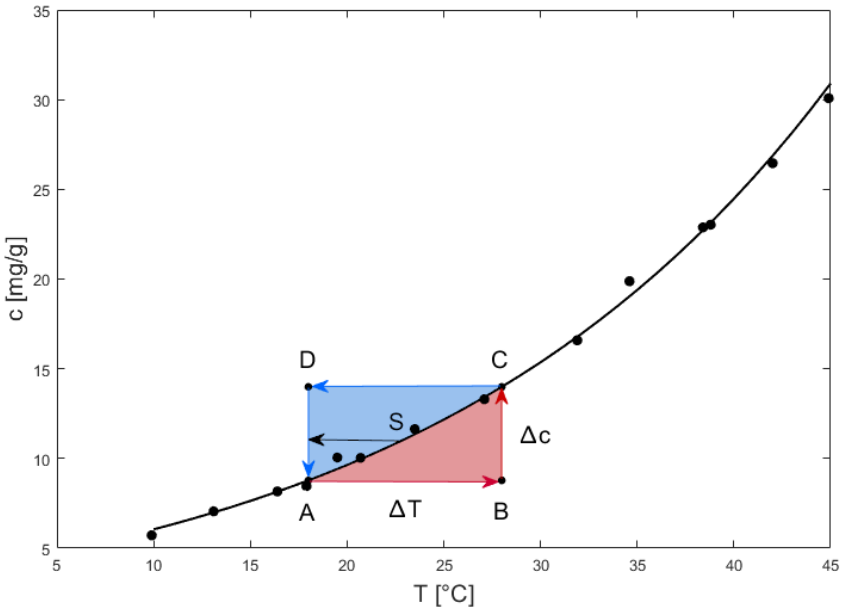

Figure 3.9: Representation of temperature and concentration change during temperature cycles in the solubility diagram of NMPA in ethanol, black dots mark the clear point temperatures, the curve is the solubility line fitted to the data, see equation (3.1), for comparison see [61].

3.4.2 Temperature variation

To get an idea for nucleation, approximately 3 g NMPA was added to about 220 g ethanol and stirred for 1 h to obtain a saturated solution. Then it was filtered and the clear solution filled in a flask and sealed with Parafilm®. The solution was transported by a peristaltic pump with a rate of 5 mL/min trough a tube immersed in two water baths held at different temperatures, whereby the warm was as much heated as the cold cooled. In several experiments, temperature differences from 2 to 22°C were realized and the product was analyzed visually for crystals. Even at the highest temperature difference no crystals could be detected and therefore, it seems that no primary nucleation took place.

3.4.3 Crystal mass variation

In a second attempt, to get an idea for the necessary dry solid mass, the saturated solution was again prepared as described before, but this time 0.5 wt% NMPA were added. The suspension was pumped through the tube with a rate of 5 mL/min, while the water baths were held at a temperature difference of 8°C, but particles blocked it in the cold water bath.

The experiment was repeated at the same pump rate with a particle amount of 0.1 wt% NMPA and this time no blocking occurred, but the NMPA amount was considered to be a too small and that 0.3 wt% would be better.

3.5 Experimental setup

For the deracemization process, a tubular reactor with a length of 48 m was used. Therefore, the 50 m long transparent silicone tube Versilic® from Roth with an outer diameter of 4 mm and an inner of 2 mm was coiled up in 12 loops in two water baths, which were held via thermostats at constant temperatures. This gave a length of 4 m per cycle, meaning that 2 m were coiled up in the cold water bath and 2 m in the warm. The residual 2 m of the tube were held at room temperature as it were not immersed in water. This resulted in a total reactor volume of

$$V = \frac{0.002^2 \cdot \pi}{4} \cdot 48 = 0.151\,\mathrm{L}. \tag{3.2}$$

A peristaltic pump was used to facilitate the transportation of the suspension through the tube, since it could not be damaged by solid particles. Directly after the pump, a syringe pump was located. The two syringes, each with a diameter of 27.63 mm and a volume of 60 mL and filled with air, were connected with two approximately 10 cm long tubes and a Y connector. Via the third opening of the Y connector and an additional tube, it was connected to a three way connector. This three way connector linked the tube from the syringes, the tube fixed to the peristaltic pump and the reactor. However, it was not connected directly to the reactor but to a 20 cm long tube to made an easier pump calibration possible. Then, the reactor immersed after 25 cm in the first water bath.

The storage round bottom flask with a volume of 1 L was located on a magnetic stirrer and connected with the peristaltic pump with a tube of 40 cm. It was, as well as both pumps, located on a lifting ramp. It was necessary for the peristaltic pump and the storage flask to ensure that no sedimentation took place and all particles were transported to the reactor. Especially between the storage flask and the peristaltic pump was a steep decline crucial, since the particles had to be transported without air. However, the syringe pump had to be located higher, to make an uniform addition of air possible.

At the end of the reactor tube, the suspension was collected in another 1 L round bottom flask. The total tube length from the flask containing the starting suspension to this collection flask were approximately 51 m. The schematic overview can be taken from figure 3.10 and a picture of the actual setup from figure 3.11.

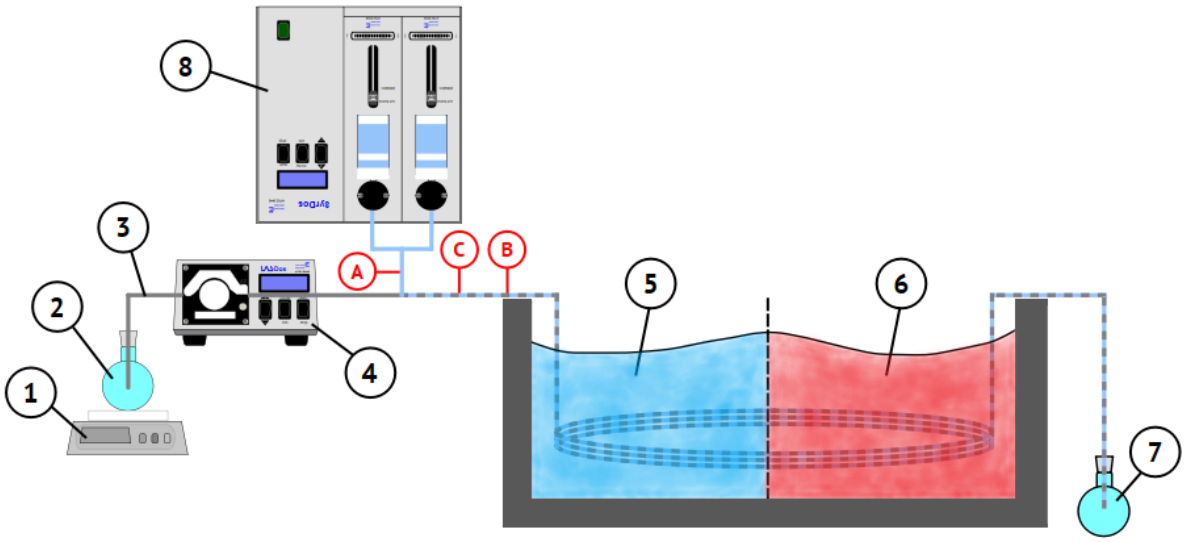

Figure 3.10: Scheme of the experimental setup, 1 magnetic stirrer, 2 starting suspension in a round bottom flask, 3 tube, 4 peristaltic pump, 5 cold water bath, 6 warm water bath, 7 suspension in a round bottom flask, 8 syringe pump, A, B and C mark spots that will be pinched off at some time during the experiment.

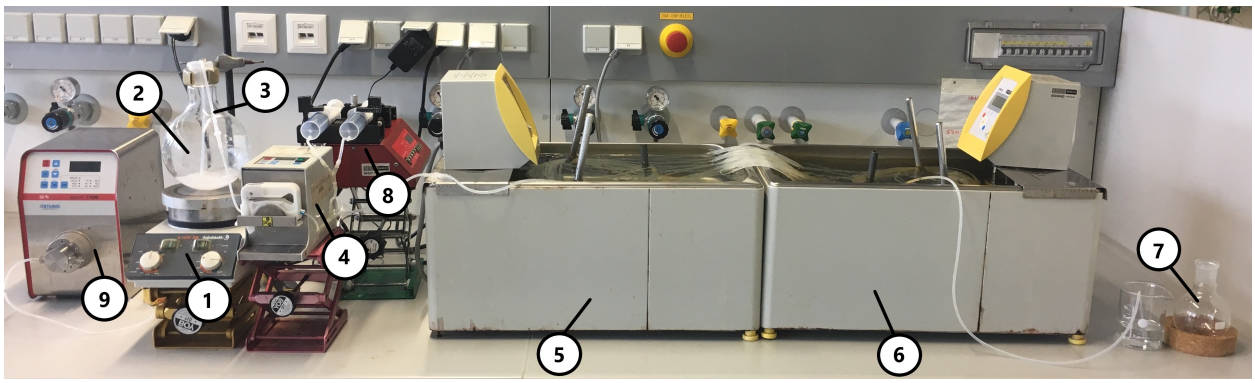

Figure 3.11: Picture of the experimental setup, 1 magnetic stirrer, 2 starting suspension in a round bottom flask, 3 tube, 4 peristaltic pump, 5 cold water bath, 6 warm water bath, 7 suspension in a round bottom flask, 8 syringe pump, 9 gear pump to enable a fast filling of the tube.

3.5.1 Setup for cycle experiments

To be able to cycle the suspension several times through the reactor, the end of the reactor was used as recycle loop. Therefore, it was connected to the beginning of the reactor and the whole suspension could be recycled. However, it was not fixed directly to the beginning but to a three way connector 30 cm after it to avoid removing the tube from the storage flask.

At the connection, two three way connectors with 3 cm tubes were installed in serial. With these connectors, the removal of air and the addition of saturated suspension with syringes with a volume of 5 mL and 60 mL was enabled.

Even though this setup enabled experiments with more cycles and therefore longer total residence times, it had the drawback that the syringe pump had to be disconnected, since it was not possible to transport air compartments by a peristaltic pump without fragmentation. Therefore, higher total flow rates had to be applied to avoid sedimentation and the residence time of a single cycle was shorter.

An overview of the setup can be taken from figure 3.12.

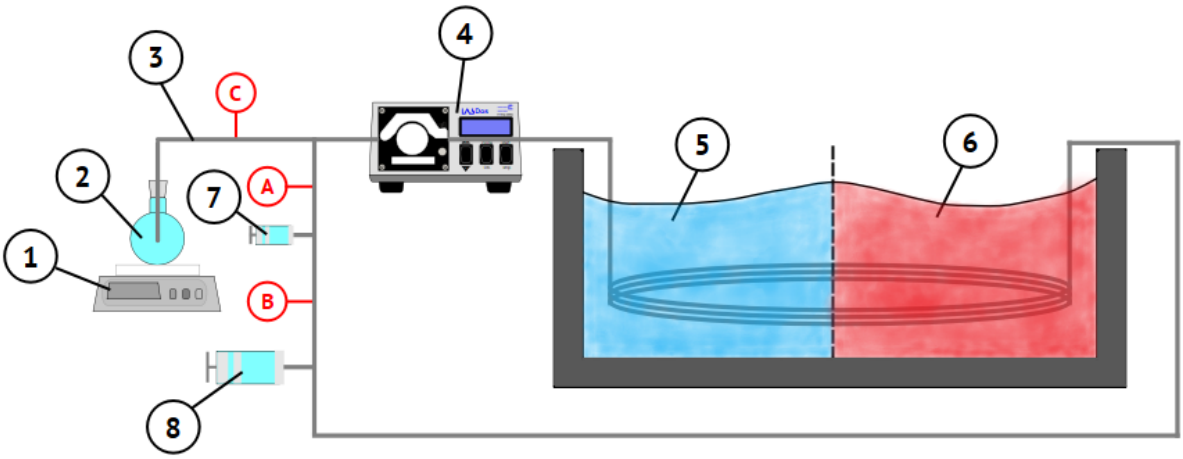

Figure 3.12: Scheme of the experimental setup for cycle experiments, 1 magnetic stirrer, 2 starting suspension in a round bottom flask, 3 tube, 4 peristaltic pump, 5 cold water bath, 6 warm water bath, 7 5 mL syringe, 8 60 mL syringe A, B and C mark spots that will be pinched off at some time during the experiment.

3.6 Experimental procedure

First of all, it was necessary to saturate ethanol with NMPA. For this purpose, approximately 1.2 g NMPA were added to about 82 g ethanol in a 1 L round bottom flask, which resulted in a visually cloudy suspension. It was stirred for at least 2 h at room temperature with a stirring bar of 5 cm to ensure sufficient mixing. Then the suspension was filtered, filled in another 1 L round bottom flask, sealed with a glass plug to avoid evaporation, and weighed. Based on this mass of saturated suspension, the amount of NMPA was calculated, whereby 0.3 wt% were used, if not declared otherwise. The total amount of crystals consisted of racemic NMPA and some enantiomerically enriched NMPA obtained from the experiments performed in the Crystalline® device, as discussed in chapter 3.3, to obtain the desired starting ee_0 of about 5 % for the experiments. This was necessary, to ensure that

every time the same enantiomer, the R-form, was favored. The crystals were weighed and added to the saturated solution, which was again stirred with a 5 cm stirring bar. About 7 mL samples were taken after 5 and 15 min with a pipette and weighed. The residual mass of the suspension corresponded to the total mass that was pumped through the reactor. Based on this, the necessary amount of the catalyst DBU, 5 $\mu L/g_{total}$ if not declared otherwise, was calculated and added. This corresponded to approximately 0.16 mol% based on the total moles of ethanol and NMPA. The latter consisted of the amount of solid NMPA present in the suspension and the dissolved NMPA. The amount of dissolved NMPA was approximated via the solubility curve for the average ambient temperature of 23 °C for the mean suspension mass of 80 g, see equation (3.1). Further, the total suspension mass could be calculated, whereby the masses of both samples had to be subtracted. For both, a mass of 5.5 g was assumed, which again corresponded to the mean of all experiments. As it was supposed that the system was homogeneously mixed, the sampling did not change the ratio of NMPA and ethanol. Therefore, the residual mass of NMPA and ethanol and further the moles could be calculated. All used substance properties are listed in the appendix 7.2

One water bath was heated and held at constant temperature by a thermostat. Ice was added to lower the temperature of the other water bath below room temperature before it was heated to the exact desired temperature by another thermostat. The addition of ice was necessary, since the used thermostats were only capable of heating. By adding more ice on times, the temperature was kept within 0.2 °C of the set temperature. If not declared otherwise, the warm water bath was as much heated as the cold cooled.

The tube had to be filled with ethanol before the experiment started, otherwise the pressure drop could change too much during the experiment as it depends on the filling degree. Therefore, the tube was not fixed in the peristaltic pump, but to a gear pump, to speed up the filling, since this pump is able to perform at higher rates. The connection to the syringe pump was pinched off at spot A to avoid flushing the syringes, see figure 3.10. As soon as the tube was filled, it was pinched off at spot B, so that the reactor could be disconnected from the residual tube at spot C without ethanol trickling from the reactor. Then, the residual tube could be emptied with the gear pump and afterwards disconnected from it and fixed to the peristaltic pump. For the calibration of the pump, water was pumped for 2 min in a beaker, weighed and the pump was adjusted until the desired flow rate was reached. Then, this part of the tube was again filled with ethanol, connected to the reactor and the pinch at spot B was detached.

Now ethanol could be pumped continuously through the tube and air was added with the syringe pump. First, the syringe pump had to pump 5 mL/min to achieve pressure equalization, before the pinch at spot A could be detached and it could be adjusted to the desired volume flow of one-fifth of the liquid volume flow of the peristaltic pump. Otherwise, the syringes would have been flushed by ethanol. For a stable process, it was furthermore necessary that all air bubbles were nearly of the same size and the fluid compartments between them as well. If the tube had not been filled before the air was added, the air could not

be added continuously, due to the high pressure drop, which was indicated by bubbles that decreased in time.

As soon as the steady state was reached and all bubbles had the same size and formed in constant time intervals, the beginning of the tube was switched from the ethanol bottle to the flask with the suspension, which was sealed by Parafilm®. After the whole suspension was pumped in the tube, ethanol was pumped through again.

1.5 min after the first particles left the reactor, the saturated solution with the crystals was collected in another flask capped with Parafilm®. Directly at the switch of the pure ethanol to the saturated solution, rarely any crystals could be detected, due to backmixing and dissolution of all crystals. Also, at the end of the experiment, the last crystals were not collected to avoid some error due to backmixing. Since the suspension was not collected at the beginning and at the end for approximately 3 min, this resulted in 24 mL discarded suspension. Then the crystals were separated by filtration, washed with cold, deionized water and dried under vacuum. They were analyzed by HPLC as soon as they were dry. The reactor was washed with pure ethanol to remove any residual NMPA.

The standard experimental settings were: water bath temperature difference: 10 °C, 5 $\mu L/g_{total}$ DBU, fluid pump rate: 4 mL/min, ratio air/fluid: 0.2, dry crystal mass: 0.3 wt%. For an ambient temperature of 23 °C, which was approximately the mean of all experiments, this resulted in a cold water bath with a temperature of 18 °C and a warm with a temperature of 28 °C. However, the temperatures were adjusted to the exact ambient temperature when saturating the ethanol with NMPA. Based on these settings, single parameters, such as the temperature difference of the water baths, amount of catalyst, pump rate and amount of solid NMPA, were changed to determine their influence on the system.

3.6.1 Recycle experiments

The preparation for the cycle experiments was the same as for the experiments described in chapter 3.6, with the exception that the tube had not to be filled with ethanol and about 60 mL more of the saturated solution had to be prepared. Then, the tube was pinched off at spot A, see figure 3.12, and the 60 mL syringe filled with saturated solution and connected to the tube. Some of the solution had to be pressed into the tube to remove the air from the connection.

The next step was to fill the tube with the suspension with use of the peristaltic pump. As soon as the whole tube was filled, the pump was switched off. The clip at spot A was detached and spot B pinched off. Then, the 5 mL syringe was connected to the tube and the remaining air sucked from the tube by spot A. Afterwards, the connection to the flask was pinched off at spot C and the clip at spot B was detached. Now it was possible to switch on the pump again. To increase the pressure and avoid degassing at the suction side of the pump, saturated solution had to be pressed into the system via the previously filled 60 mL

syringe. Since ethanol diffuses continuously through the tube wall, this had to be repeated every few minutes.

To end the experiment, spot C was again detached, spot A pinched off and the 5 mL syringe removed, to be able to empty the tube. The suspension was collected in a flask, similar to the other experiments.

4 Results

The experiments confirmed that a deracemization of NMPA during flow is possible. Since the initial enantiomeric excess was not constant, as already discussed in chapter 3.3.1, the cycle number based deracemization constant

$$k_N = \frac{1}{N} \cdot \ln\left(\frac{ee}{ee_0}\right) \tag{4.1}$$

was used, see equation (2.5), to compare the experiments. Obviously, the further advanced the deracemization is per cycle, the higher is k_N. This constants and the measured enantiomeric excesses of all experiments can be taken from the appendix 7.4.

4.1 Influence of particle size

Since the mechanism of the deracemization during temperature cylces are dissolution of small particles and agglomeration [8], one suspects that the crystals grow during the temperature cycles in the Crystalline® device. Therefore, the enantiomerically enriched crystals should have a larger mean particle size than the racemic, which was confirmed by microscopy, see figure 4.1.

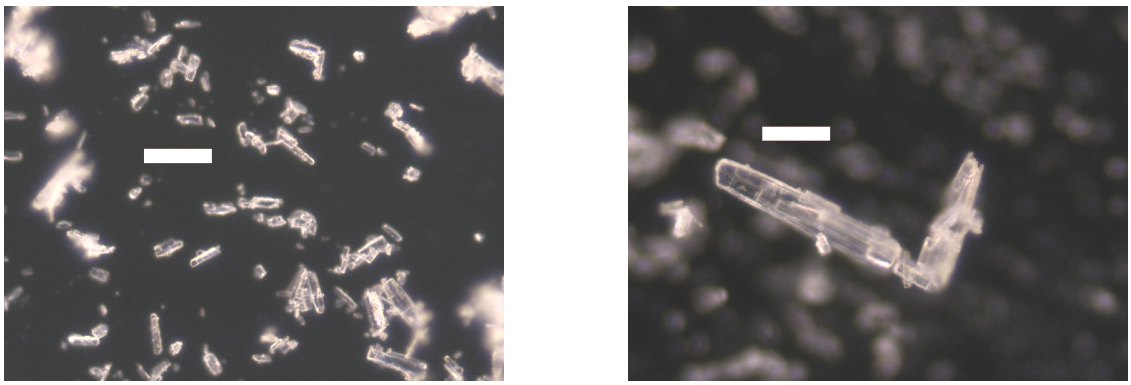

Figure 4.1: Microscopic picture of not ground NMPA before forced to temperature cycles (left picture) and afterwards (right picture), white bar indicates a length of 50 µm.

For investigating the influence of different crystal sizes, experiments with ground and not ground particles were performed. Since either the racemic or the enantiomerically enriched NMPA can be ground, this resulted in four possible combinations and, as each experiment

was performed twice, eight experiments. All experiments were performed with standard conditions and the initial enantiomeric excesses, obtained excesses and the deracemization constants can be taken from table 4.1. One has to notice that as soon as the suspension of the experiment E2 was leaving the reactor it was collected for a few minutes and the rest separately, to get an idea for backmixing, see chapter 4.2. Additionally, at the experiment E3 the suspension was collected in three terms. The values in table 4.1 correspond only to the second sample of E2 and the middle sample of E3.

Table 4.1: Experiments 1-8, 48 m tubular reactor, coiled up in 12 cycles ($N = 2$), water bath temperature difference: 10 °C, 5 µL/g_{total} DBU, fluid pump rate: 4 mL/min, ratio air/fluid: 0.2, dry crystal mass: 0.3 wt%, mean *ee* of two samples at the beginning, *ee* at the end determined by chiral HPLC and number based deracemization constant, influence of grinding, enant. stands for enantiomerically

notation	ee_0 [%]	*ee* [%]	k_N	specification
E1	9.377	31.388	0.101	no crystals are ground
E2	13.763	31.578	0.069	no crystals are ground
E3	12.350	38.944	0.096	racemic crystals are ground
E4	13.311	18.224	0.026	racemic crystals are ground
E5	13.068	39.800	0.093	racemic and enant. enriched crystals are ground
E6	13.643	35.834	0.080	racemic and enant. enriched crystals are ground
E7	10.897	32.498	0.091	enant. enriched crystals are ground
E8	8.842	27.086	0.093	enant. enriched crystals are ground

One can see that the results from the experiments E5-E8, when the enantiomerically enriched crystals were ground, are more reproducible, which confirms that it has an influence on the experiments, if some crystals are present in the system that exceed the others in size. It seems that the symmetry is harder to break if some of both, the R and S crystals, are bigger, so both enantiomers are hard to dissolve and have a big surface for agglomeration. If the added crystals would have not only been enantioenriched but enantiopure, it may be that there is no need for grinding. However, one needs to be aware that the deracemization is slower if they are too big, see chapter 2.4.2.

However, as can be seen in figure 4.2, grinding of the particles with mortar and pestle did not result in perfect homogeneity in size. Some crystals were still nearly as big as the racemic and it may be that the small dissolved during the experiments E7-E8 and the difference of the remaining enantiomerically enriched crystals to the racemic was not significant. Therefore, the symmetry would have been also harder to break if some of the crystals of the racemate had a bigger size. Due to this, in the following the enantiomerically enriched crystals as well as the racemat were ground, as was done in the experiments E5-E6.

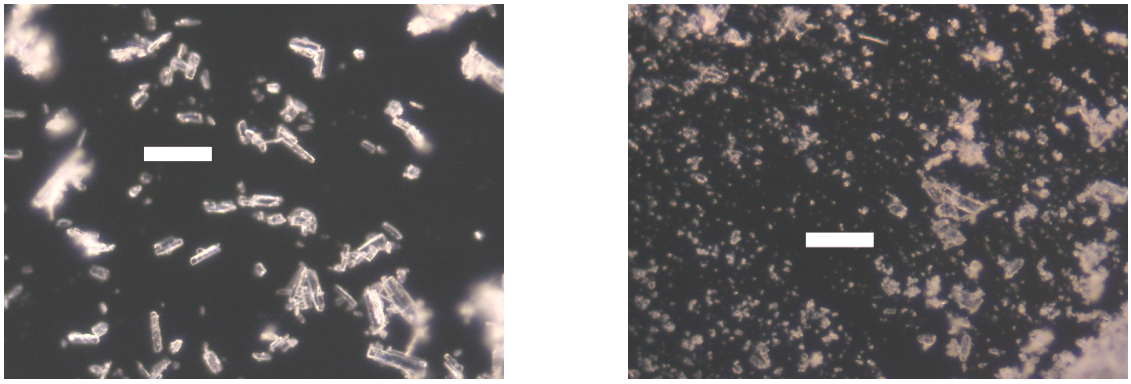

Figure 4.2: Microscopic picture of not ground racemic NMPA (left picture) and ground enantiomerically enriched NMPA (right picture), white bar indicates a length of 50 µm.

4.2 Backmixing

The experiment E9 was also performed with the standard settings, whereby all crystals were ground. Similar to the experiment E3, the suspension leaving the reactor was collected in three terms, each 4 min long. The obtained enantiomeric excesses of the experiments E2, E3 and E9 were related to the mean of the initial enantiomeric excesses of the two samples at the beginning of the experiment via the deracemization constant k_N and listed in table 4.2.

Table 4.2: Experiments E2, E3 and E9, 48 m tubular reactor, coiled up in 12 cycles, water bath temperature difference: 10 °C, 5 µL/g_{total} DBU, fluid pump rate: 4 mL/min, ratio air/fluid: 0.2, dry crystal mass: 0.3 wt%, k_N values were calculated with the mean *ee* of two samples at the beginning, influence of backmixing

notation	k_{N1}	k_{N2}	k_{N3}
E2	0.044	0.069	-
E3	0.068	0.096	0.056
E9	0.063	0.109	0.057

As can be seen, the k_N value is higher in the middle of each experiment, indicating a further advanced deracemization. Since before and after the suspension ethanol was pumped through the tube, the smaller deracemization constants at the beginning and the end of the experiments could be an indication for backmixing. Due to the backmixing, more ethanol is present in the system, enabling additional crystals to dissolve. The suspicion is also confirmed by the fact that in the first few milliliter of suspension no crystals could be detected. Therefore, the sample taken at the middle of the experiment should be the most representative for the steady state performance of the reactor.

4.3 Influence of parameters

In the following, the influence of some parameters on the experimental outcome of the deracemization in a tubular reactor is discussed. The temperature difference, amount of catalyst, residence time and amount of solid crystals were investigated. The process depends also on the initial enantiomeric excess, since the reaction is autocatalytic, the heating and the cooling rate, which was already discussed in chapter 2.4.2.

Each experiment was performed with ground crystals twice in terms of better reproducibility and the mean of the cycle number based deracemization constants k_N was calculated. This constants were used for the comparison of experiments with different settings. Nonetheless, care has to be taken, since the deracemization experiments are sensitive to initial conditions [43, 57, 74] and the starting suspension was up to a certain degree not homogeneously mixed, giving spatially fluctuations of the enantiomeric excess. Of all experiments, the mean value of the differences of the *ee* of the two samples from the starting suspension is about 1.3 %, but for some it is as high as 3 %.

It has to be mentioned that at one of the two performances of the experiment with the standard settings, the suspension was three times for 4 min collected, to get an idea for backmixing, and only the result of the middle sample is discussed in the following.

4.3.1 Temperature difference

Different temperatures could easily be realized via the two water baths. As can be seen in figure 4.3, the number based deracemization constant increases linearly for temperature swings from 0.036 at 2 °C to 0.143 at 12 °C. It has to be noted that at one experiment with $\Delta T = 2\,°C$, a difference of the enantiomeric excesses of 5.088 % was measured between the two samples of the starting suspension. However, it shows that high temperature swings accelerate the deracemization. The same trend was observed by other groups, as the higher the temperature swing, the more crystals are involved in dissolution and recrystallisation [8, 20]. At the differences of 24 °C and 29 °C, one has to notice that the warmer water bath was not as much heated as the colder cooled. At this experiments, it was 6 °C warmer than the ambient temperature and the other 18 °C, respectively, 23 °C colder. Anyhow, it can be seen that the linear trend is not continued for this large temperature swings, giving an optimum. Since the probability of secondary nucleation is bigger at higher temperature differences [75], it is likely that it occurred at the differences of 24 °C and 29 °C and slowed down the process due it's stochastic nature [75].

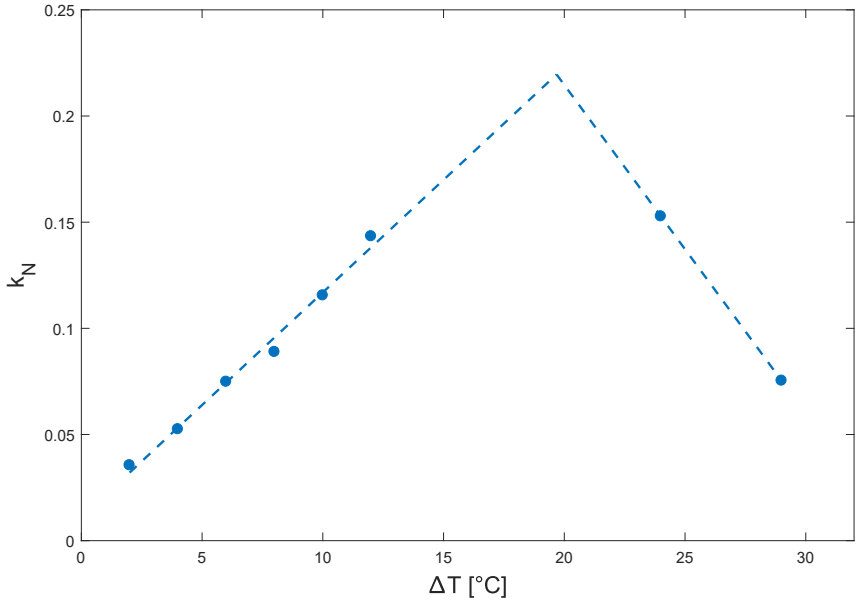

Figure 4.3: Cycle number based deracemization constant for NMPA in ethanol at various water bath temperature differences, in a 48 m tubular reactor, coiled up in 12 cycles, 5 µL/g_{total} DBU, fluid pump rate: 4 mL/min, ratio air/fluid: 0.2, dry crystal mass: 0.3 wt%, mean value of two experiments, the lines are drawn to guide the eye.

For optimizing the process, more experiments are required with a temperature difference between 12 °C and 24 °C to detect the optimal temperature swing. However, especially for industrial applications, the optimal conditions do not necessarily have to result in the highest k_N value, which would mean a high probability of secondary nucleation. Also, due to the stochastic nature of the nucleation, the process would not lead to reproducible results. Moreover, the higher the temperature difference is, the higher is the demand of energy to heat, respectively, cool the water baths.

For further optimization of the process, it might also be beneficial to use damped temperature cycles. It was already proven that the total deracemization time of batch experiments can be reduced if first high temperature differences are used to break the symmetry and then smaller ones [43]. Therefore, the cycles have to get shorter, if applied to the tubular reactor. However, it has to be mentioned that the continuous process is faster than the batch, see chapter 4.3.8, and it is not given that it can be further accelerated by using damped cycles.

4.3.2 Catalyst amount

In figure 4.4, the dependence of k_N on the catalyst amount can be seen. The process can be accelerated by higher amounts of DBU, as the deracemization constant increases from 0.092 with 1 µL/g_{total} DBU to 0.147 with 7 µL/g_{total}. It can also be seen that the incline of

the slope is steeper for higher catalyst amounts, whereby it once again has to be mentioned that the experiments are sensitive to the initial conditions. Especially one sample of the initial suspension at one experiment with 1 $\mu L/g_{total}$ is not representative, since only a small amount of crystals was in the sample suspension and only 0.7 mg could be analyzed by the HPLC.

A higher amount of catalyst accelerating the deracemization was also observed by Noorduin et al. [76]. One reason for this could be the faster racemization reaction, as it is likely that if the reaction is too slow, the concentration difference between the enantiomers in solution could not be balanced. Another reason that the solubility of the crystals is increased and therefore more crystals are involved per cycle [20].

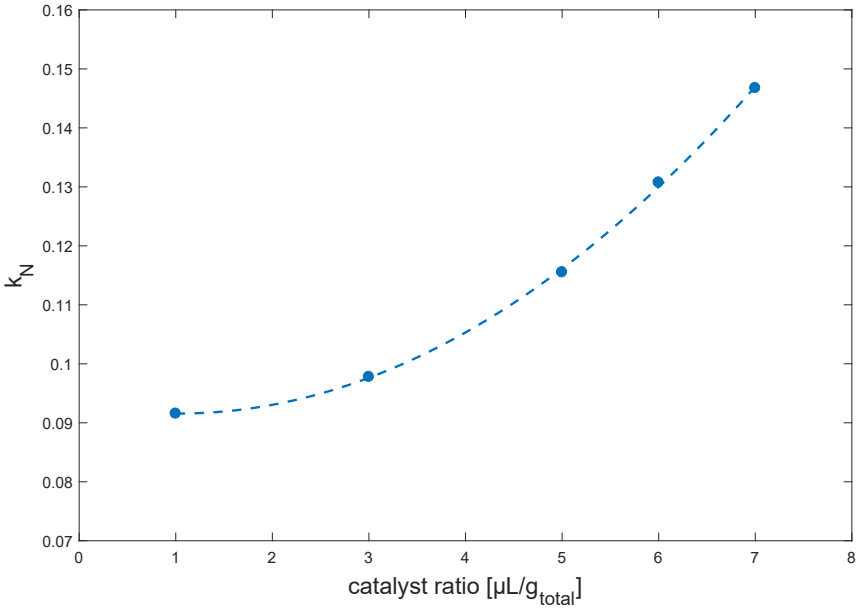

Figure 4.4: Cycle number based deracemization constant for NMPA in ethanol with various amounts of DBU in a 48 m tubular reactor, coiled up in 12 cycles, water bath temperature difference: 10 °C, fluid pump rate: 4 mL/min, ratio air/fluid: 0.2, dry crystal mass: 0.3 wt%, mean value of two experiments, the line is drawn to guide the eye.

Since the curve does not flatten out at high amounts of DBU, it is indicated that the deracemization process could be further accelerated by adding more catalyst. However, to determine the optimal catalyst amount, more experiments are necessary, as it is likely that at some point so much catalyst is present that the deracemization is not further accelerated when adding more.

4.3.3 Residence time

One possibility for the realization of different resident times is via variation of the total reactor length, whereby either more or longer cycles can be used to extend the reactor. Obviously, the more cycles are used, the further advanced is the deracemization at the end, as it is an autocatalytic reaction, see chapter 2.4.2. However it was shown by Suwannasang et al. that increasing the number of cycles does not influence the deracemization rate per cycle and only makes sense until full deracemization is reached [8]. Contrary, it is possible to change the deracemization progress per cycle via variation of the cycle length, though only until the system reaches equilibrium, see chapter 2.4.2. Any further extension of the cycles, which results in longer isothermal periods, has no influence on the process [8].

Another possibility to change the residence time is via the flow rate of the suspension. If the system is considered ideal and no backmixing occurs, the effects on the system are assumed to be similar to these when using longer cycles. In the following, the influence of the flow rate is investigated, whereby the ratio of the suspension volume flow to the air volume flow of 0.2 is kept constant. As can be taken from figure 4.5, the deracemization constant decreases with a higher volume flow, meaning a shorter residence time, from 0.116 at 4 mL/min to 0.097 at 10 mL/min. This indicates that the time needed to reach equilibrium was longer than the residence time of the suspension in each water bath.

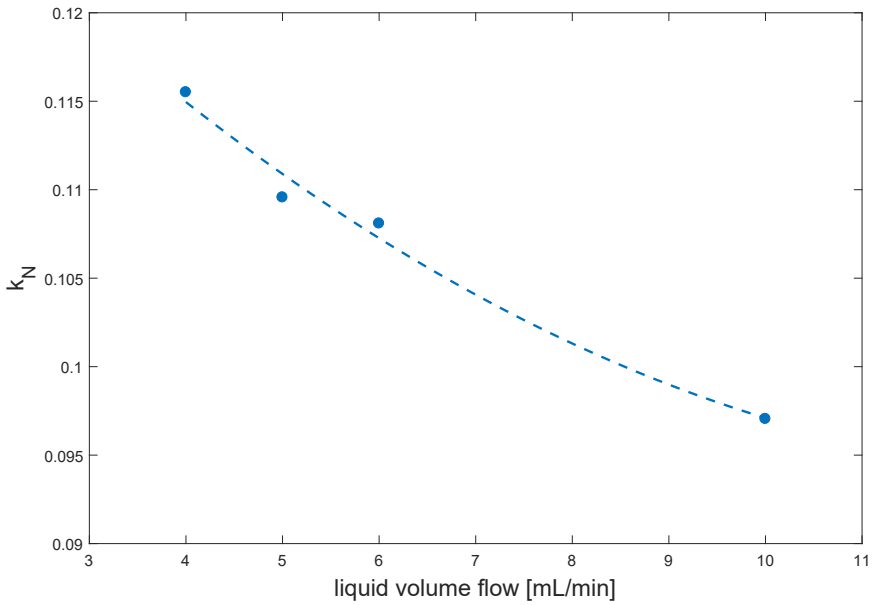

Figure 4.5: Cycle number based deracemization constant for NMPA in ethanol for various pump rates, in a 48 m tubular reactor, coiled up in 12 cycles, water bath temperature difference: 10 °C, 5 µL/g_{total} DBU, ratio air/fluid: 0.2, dry crystal mass: 0.3 wt%, mean value of two experiments, the line is drawn to guide the eye.

The pump rate of 4 mL/min, leading to the highest k_N, is already quite small and can not be decreased any more to avoid sedimentation. However, it may be reasonable to test if the experiment can still be performed with 3 mL/min, but it has also to be considered that this extends the total process time. Calculating the cycle volume using the reactor volume, see equation (3.2),

$$V_{cycle} = \frac{V}{12} = 0.0503\,\mathrm{L}, \tag{4.2}$$

the time necessary to complete one cycle can be estimated for various pump rates. Furthermore, with the observed deracemization constants, the required number of cycles to reach enantiomeric purity can be calculated using equation (2.5), if the experiments are started with an ee_0 of 18 %. This initial enantiomeric excess was chosen, to make the results comparable with the batch experiments of Breveglieri et al. [61], see chapter 4.3.8. The evolution of the excesses during the cycles for the various pump rates can be seen in figure 4.6.

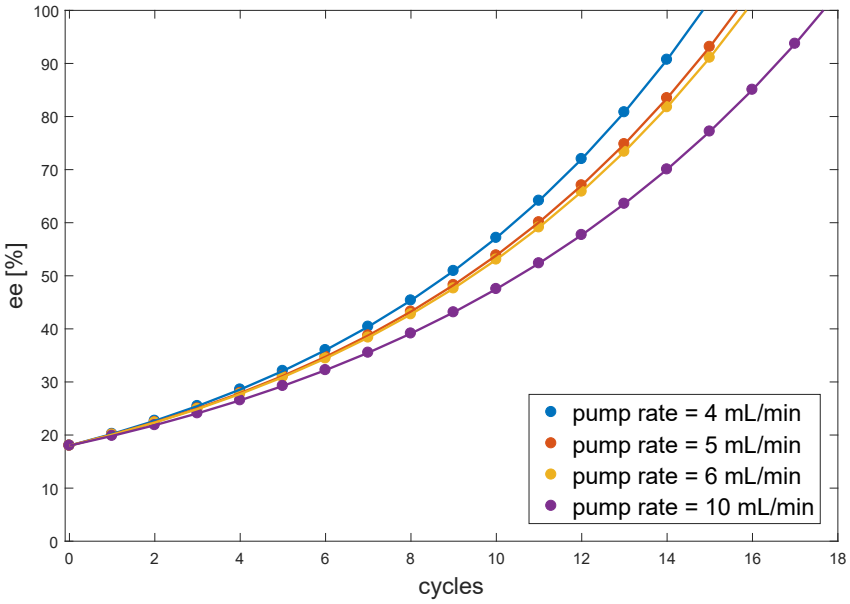

Figure 4.6: Estimated evolution of *ee* per cycle for the deracemization of NMPA in ethanol in a 48 m tubular reactor, water bath temperature difference: 10 °C, 5 $\mu L/g_{total}$ DBU, ratio air/fluid: 0.2, dry crystal mass: 0.3 wt%, the calculation is based on k_N observed in experiments.

Multiplication of the required number of cycles with the time necessary to complete one cycle gives the total process time, neglecting the time required to transport the crystals to the reactor. The results are summarized in table 4.3.

Table 4.3: Calculated necessary time to complete 1 cycle, calculated required number of cycles and calculated total process time for the deracemization of NMPA in ethanol for various pump rates with an ee_0 of 18 %, the calculations were performed with the cycle number based deracemization constants observed in a 48 m tubular reactor, coiled up in 12 cycles, water bath temperature difference: 10 °C, 5 $\mu L/g_{total}$ DBU, ratio air/fluid: 0.2, dry crystal mass: 0.3 wt%, mean value of two experiments

pump rate [mL/min]	k_N	t_{cycle} [min]	cycles	t_{total} [min]
4	0.116	3.14	15	47.12
5	0.110	2.51	16	40.21
6	0.108	2.09	16	33.51
10	0.097	1.26	18	22.62

As can be seen, the total process is faster using high pump rates although the deracemization per cycle is further advanced with low pump rates. The time required to reach enantiomeric purity using a pump rate of 4 mL/min is 24.5 min longer than with a pump rate of 10 mL/min. This shows that the time required for the additional cycles to reach enantiomeric purity is shorter than the time needed for longer cycles.

Therefore, if optimizing an industrial process, high pump rates and long reactors might be desired. However, it has to be considered that both parameters are limited. For example it was observed that at a pump rate of 16 mL/min it was not possible to achieve a stable slug flow as the air was not added uniformly. Furthermore, the length of the reactor could only be extended until the pressure drop of the tube is too high to be overcome by the pump, see chapter 2.5. Even though no difficulties were observed during pumping the suspension through the 50 m long tube and it is also expected that there are none when using 15 cycles, which corresponds to 60 m, more experiments are required to investigate if also 72 m in 18 cycles can be used.

4.3.4 Crystal mass

Last but not least, figure 4.7 shows the dependence of the deracemization constant on the dry solid mass. A higher solid mass slows down the process, as the constant decreases from 0.116 at 0.3 wt% to 0.049 at 1 wt%. The inversely proportional behavior of the deracemization rate to the suspension density was also shown in other experiments [8, 20, 76]. This is due to the smaller amount that has to deracemize and also to the higher percentage of solid crystals dissolving and recrystallizing in each cycle [8].

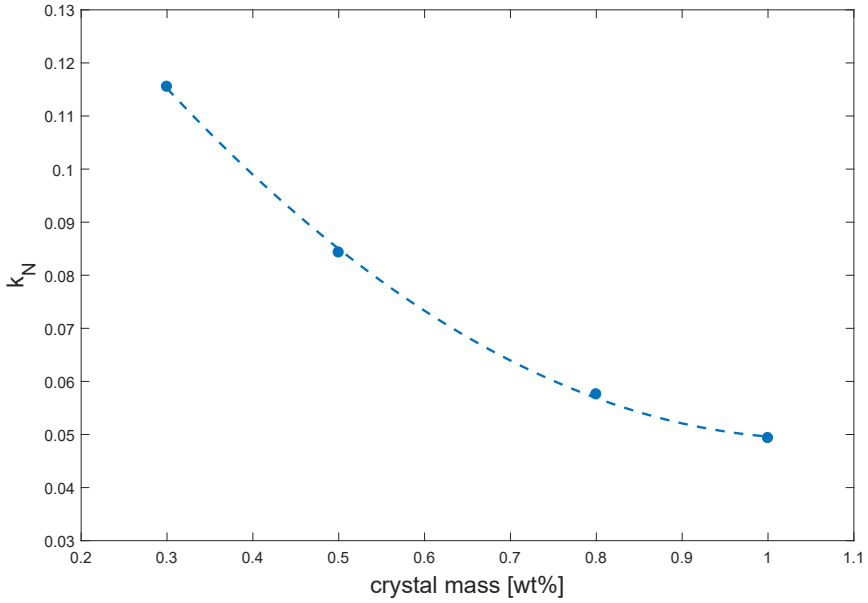

Figure 4.7: Cycle number based deracemization constant for NMPA in ethanol at various dry crystal masses, in a 48 m tubular reactor, coiled up in 12 cycles, water bath temperature difference: 10 °C, 5 µL/g_{total} DBU, fluid pump rate: 4 mL/min, ratio air/fluid: 0.2, mean value of two experiments, the line is drawn to guide the eye.

For the experiments, typically 80 g of saturated solution were used. When using 0.3 wt% it corresponds to 0.24 g NMPA, which is already quite small. For 0.2 wt%, only 0.16 g solid NMPA are involved, so further decreasing the crystal amount might not be sufficient. Therefore, for industrial applications it is better to choose a low k_N, like 0.049 at 1 wt% or 0.058 at 0.8 wt%, and improve the process via other parameters.

4.3.5 Productivity

Generally, the productivity is defined as the solid mass m produced per volume of the crystallizer V and the total time t_{total} [77]

$$P = \frac{m}{V \cdot t_{total}}. \tag{4.3}$$

However, if the process is performed with an initial enantiomeric excess, the term has to be multiplied with the half difference of the enantiomeric excess at the end and the beginning [61]

$$P = \frac{m}{V \cdot t_{total}} \cdot \left(\frac{ee - ee_0}{2}\right). \tag{4.4}$$

For the estimation of the deracemization productivity in the tubular reactor, it was assumed that the ambient temperature was constant during the experiments. Therefore, the solubility of NMPA in ethanol before and after the experiment was the same and the mass of the solid produced corresponded to the mass of solid NMPA initially added to the saturated solution. Moreover, the density of the solution was assumed to be the density of pure ethanol when calculating the volume from the total mass of about 80 g. For the density see the appendix 7.2. The cycles and process time necessary for complete deracemization when starting with an ee_0 of 18 % can be taken from chapter 4.3.3. All calculations were done with the mean of two experiments performed with the same settings for better reproducibility, similarly to the estimation of the deracemization constants. The exact values can be taken from the appendix 7.5.

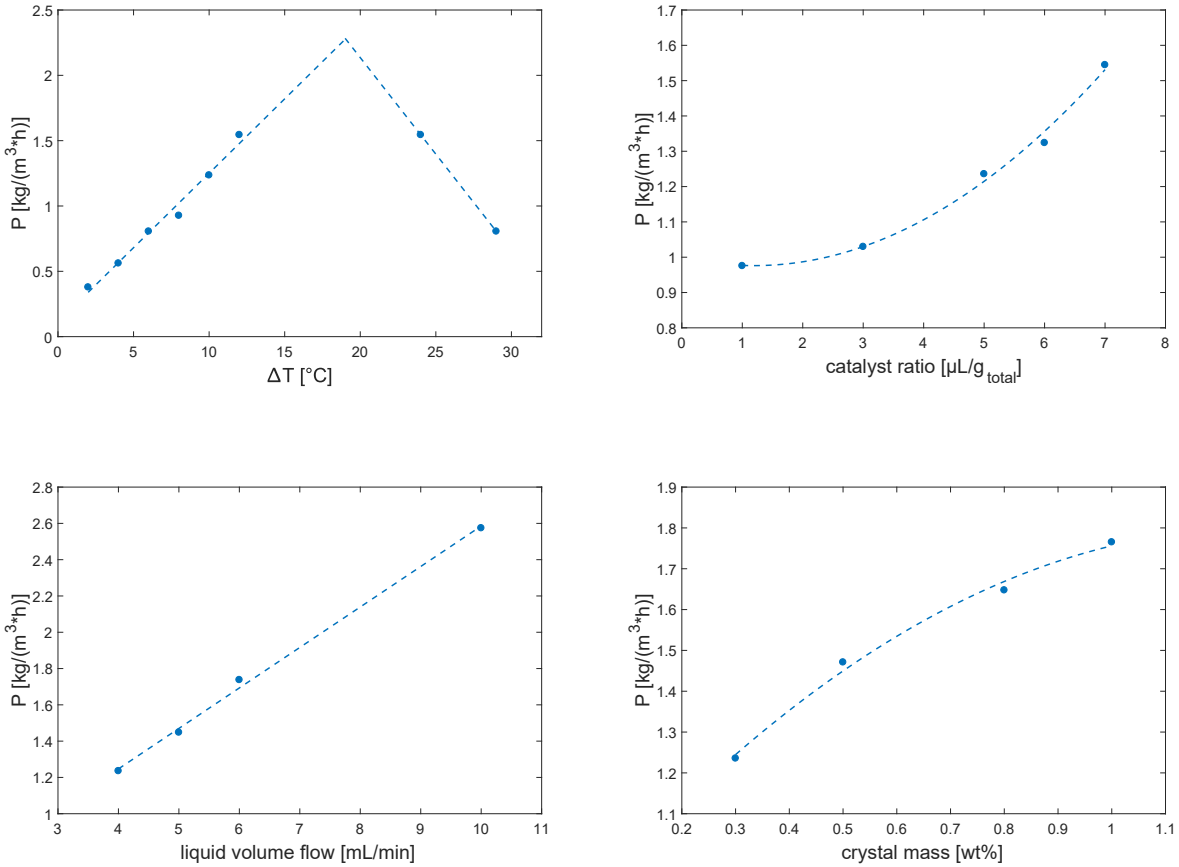

Figure 4.8: Calculated productivity of the deracemization of NMPA in ethanol, 48 m tubular reactor, coiled up in 12 cycles, ee_0: 18 %, comparison of influence of water bath temperature difference, catalyst amount, fluid pump rate and crystal mass, the lines are drawn to guide the eye.

As can be seen in figure 4.8, the dependence of the productivity on the temperature difference and the catalyst amount is similar to the dependence of the deracemization constant k_N on these parameters. This confirms that the productivity can be increased via a high

deracemization rate per cycle. Contrary, the productivity is indirect proportional to the dependence of the k_N on the liquid flow rate and the crystal mass. As already discussed, a faster process, respectively, a higher mass is beneficial for an industrial application and should be chosen as long as other parameters can be varied to reach enantiomeric purity.

4.3.6 Comparison of the influence of the parameters

In table 4.4, for each parameter study the biggest experimentally obtained number based deracemization constant k_N, the productivity P as well as the greatest changes are listed. The greatest changes were calculated as difference of the biggest observed values and the smallest.

Table 4.4: Cycle number based deracemization constant and productivity for NMPA in ethanol, 48 m tubular reactor, coiled up in 12 cycles, comparison of influence of water bath temperature difference, catalyst amount, fluid pump rate and dry crystal mass, mean value of two experiments

max k_N	Δk_N	max P [kg/(m^3·h)]	ΔP [kg/(m^3·h)]	parameter varied
0.153	0.117	1.545	1.166	temperature difference
0.147	0.055	1.545	0.569	catalyst amount
0.116	0.018	2.574	1.339	pump rate
0.116	0.066	1.765	0.530	crystal mass

It can be seen that the best result with a k_N of 0.153 was achieved via optimizing the temperature difference. Since Δk_N is also the biggest and ΔP the second biggest value, the deracemization process seems to be sensitive to the temperature difference and can be easily adapted with this. However, as already discussed, there is not much space for improvement left, whereby via the catalyst amount no limit was detected yet. Since the k_N of 0.147 is not much smaller, it is likely that the process can be even further accelerated via the catalyst amount than via the temperature difference.

The pump rate has the least influence on the deracemization per cycle, since an increase of 6 mL/min only resulted in a Δk_N of 0.018. However, it has the biggest influence on the productivity. The pump rate of 10 mL/min resulted not only in the highest P of 2.574, via the variation was also the biggest change of 1.339 achieved, indicating that the process is most sensitive to the pump rate in the observed parameter ranges. Therefore, as already discussed, for further optimization it is better to change the amount of cycles and use high pump rates.

Optimization of the deracemization per cycle via the crystal mass is also restricted, as 0.3 wt% (0.24 g) is already a small amount and any further decreasing results in a smaller yield. However, as can be seen at the second biggest P of 1.765, the crystal mass can be

increased to achieve a higher yield as long as the process can be adapted via the other parameters to reach enantiomeric purity.

Therefore, the biggest cycle number based deracemization constant seems to be at a temperature difference a bit higher than 12 °C, a pump rate of 4 mL/min, 0.3 wt% crystal mass and a high catalyst amount, whereas more experiments are necessary to determine the optimum. However, for the best process conditions, a higher pump rate and more crystal mass should be used.

4.3.7 Percentage of NMPA involved per cycle

Via the solubility curve of NMPA in ethanol, see chapter 3.4.1, the amount of NMPA which dissolves and recrystallizes per cycle can be estimated. Therefore, the maximum concentration of solid NMPA present at the lowest temperature during the process can be calculated as sum of the solid NMPA added to the saturated solution and the NMPA crystallizing during the cooling period. For simplification, the ambient temperature was assumed to be 23 °C, which corresponds approximately to the average of all experiments. Similarly, the concentration at the highest temperature can be calculated, whereby the amount which dissolves has to be subtracted. Since no negative values can be obtained as no more crystals can dissolve as those present, negative values were set to zero.

Finally, the total concentration change per cycle can be calculated as the difference between the concentrations at the lowest and highest temperature and related to the maximum amount of solid crystals present in the system. For the experiment with the standard settings, this gives 100 %. The results for other temperature differences, respectively, other crystal masses can be taken from tables 4.5 and 4.6.

Table 4.5: Calculated percentage of NMPA involved in each cycle related to the total amount of NMPA at the deracemization in ethanol at various water bath temperature differences, in a 48 m tubular reactor, coiled up in 12 cycles, 5 $\mu L/g_{total}$ DBU, fluid pump rate: 4 mL/min, ratio air/fluid: 0.2, dry crystal mass: 0.3 wt%, mean value of two experiments

ΔT [°C]	% NMPA
2	52.61
4	86.04
6	100
8	100
10	100
12	100

Table 4.6: Calculated percentage of NMPA involved in each cycle related to the total amount of NMPA at the deracemization in ethanol at various dry crystal masses, in a 48 m tubular reactor, coiled up in 12 cycles, water bath temperature difference: 10 °C, 5 µL/g_{total} DBU, fluid pump rate: 4 mL/min, ratio air/fluid: 0.2, mean value of two experiments

crystal mass [gew%]	% NMPA
0.3	100
0.5	100
0.8	89.44
1	76.83

Since during all experiments crystals could be detected, obviously the system could not reach equilibrium when 100 % should be dissolved, see chapter 2.4.2. However, at the smaller temperature differences of 2 °C and 4 °C, it might be that the equilibrium was reached.

4.3.8 Comparison with batch experiments

As already mentioned, the highest k_N of 0.153 was achieved at a temperature difference of 24 °C, 5 µL/g_{total} DBU, a pump rate of 4 mL/min, an air/fluid ratio of 0.2 and 0.3 wt% crystal mass. The fastest experiment leading to a k_N of 0.097 and to the highest P of 2.547 kg/(m^3·h) was performed at the same conditions, only differing in the smaller temperature difference of 10 °C and the higher pump rate of 10 mL/min.

The required number of cycles and the total reactor volume to reach complete enantiomeric purity can be calculated for both experiments with the equations (2.5) and (4.2), when starting with an assumed initial enantiomeric excess of 18 %. Considering the reactor volume and pump rate, also the process time for suspension volumes smaller or equal the reactor volume and for 1 L can be calculated. The results are summarized in table 4.7. Note has to be taken that the time to transport the crystals to the reactor was neglected.

Table 4.7: Calculated required amount of cycles, calculated required reactor volume V, calculated total process time, calculated process time for 1 L suspension and calculated productivity (see chapter 4.8) for the deracemization of NMPA in ethanol with an ee_0 of 18 %, the calculations were performed with the the cycle number based deracemization constant observed in a 48 m tubular reactor, coiled up in 12 cycles, water bath temperature difference: 24 °C, 5 µL/g_{total} DBU, fluid pump rate: 4 mL/min, ratio air/fluid: 0.2, dry crystal mass: 0.3 wt%, respectively, for the same conditions but temperature difference: 10 °C, pump rate: 10 mL/min, mean value of two experiments

pump rate [mL/min]	k_N	cycles	V [L]	t_{total} [min]	t_{1L} [min]	P [kg/(m^3·h)]
4	0.153	12	0.603	37.70	250	1.545
10	0.097	18	0.905	22.62	100	2.574

As can be seen, is the deracemization rate per cycle at temperature swings of 24 °C not high enough to shorten the total process time as much as the high pump rate of 10 mL/min. Even though only 12 cycles are required, instead of 18, the total process time is 15.08 min longer, due to the longer cycle times. At the experiment with the pump rate of 10 mL/min, total resolution of 10 mL can be achieved after 22.62 min, which is about 3.5 h faster than what was observed in a batch experiment [61]. Furthermore, the productivity of this experiment is about 0.560 kg/(m^2·h) higher than the productivity of the batch experiment, which was calculated with 2.014 kg/(m^2·h) according to chapter 4.8, using the experimental data from Breveglieri et al. [61]. However, care has to be taken, because for this comparison the fastest batch experiment was chosen and the parameters differ from the continuous experiment. For the batch experiment a mixture of isopropanol and acetonitril (95/5 w/w), less catalyst with 3.85 µL/g_s, a higher crystal mass of 2.5% g/g_s and a temperature difference of 11.3 °C were used.

However, it has to be considered that in the continuous experiment more suspension has to be used, since backmixing will occur. If 24 mL are discarded, see chapter 3.6, this results in a necessary total suspension volume of 34 mL. Considering the total reactor volume of 0.151 L this has no influence on the total process time. Additionally, it has to be mentioned that a suspension volume of 10 mL is small and it would be better to perform experiments with more suspension anyway. If 1 L would have been used, a process time of 100 min is required.

4.4 Recycle experiments

A recycle experiment was performed for 2 h with a water bath temperature difference of 10 °C, 5 µL/g_{total} DBU, a fluid pump rate of 10 mL/min and a crystal mass of 0.3 wt%. An *ee* of 5.05 % was achieved when starting with 2.02 %. It has to be mentioned that the result might not be representative, as the starting suspension was in a 250 mL flask and the mixing

was not sufficient. Yet it still shows that this might be an industrially relevant alternative to the addition of air bubbles, if more research work is done, even if it has the drawback that no entire continuous process is possible. However, for longer residence times, bigger tubes might be necessary, as the crystals blocked the tube in a second experiment under the same conditions within 3 h.

5 Improvements

According to the obtained results, the following improvements of the process are suggested. Additionally, a possibility to further increase the deracemization constant is introduced, which was not tested yet.

It is likely that during filtration, washing and drying of the NMPA for the starting suspension, which was enantiomerically enriched in the Crystalline® device, a racemization reaction took place, as already discussed in chapter 3.3.1. Filtration and washing took about 15 min and the crystals needed 2 days in the desiccator to dry completely, whereby the desiccator had to be opened from time to time to exchange wet air. Even though the amount of crystals obtained from the experiments was smaller, it seems necessary to assume that a racemization reaction took place as well. Filtration and washing took still 10 min and drying 1 day. It would be possible to test this if the crystals were analyzed by chiral HPLC directly after the experiments, but we wanted to ensure that the catalyst was removed before the measurement. Further, the crystals had to be completely dry to avoid damaging the chiral column with water. However, it would be possible to overcome this by accelerating the drying process via an oven instead of a desiccator. However, care has to be taken that the oven is not too hot to avoid decomposition and racemization of the NMPA. Additionally, it might be beneficial to remove the crystals from the filter paper before drying and to ensure that no big clusters are present. Another possibility would be to perform the filtration under vacuum instead of performing a gravity filtration, to speed it up. This would also result in less residual moisture at the crystals and a shorter drying time.

Moreover, after grinding with mortar and pestle still significant differences of the crystal sizes were present. As the process was influenced by different particle sizes, see chapter 4.1, it might be better to use a mill to overcome any inhomogeneities in size.

It would also be beneficial to optimize the amount of suspension that has to be discarded at the beginning and the end of the experiment. This could be done for example via separately collecting the suspension after the tube for time intervals of 1 min. If these samples were analyzed, the time until the first sample with an *ee* that is considered sufficient could be determined. Another possibility would be the classification of the backmixing behavior of the reactor. For example, the residence time distribution could be determined by using a tracer [71].

As already mentioned in chapter 2.4.1, there are several possibilities to favor one enantiomer and obtain the desired chiral end state. In this master's thesis, an initial enantiomeric excess

was induced before starting the experiments. However, for industrial applications it might be more beneficial not to manually enrich one enantiomer, but to use a partial recycle reactor. Therefore, some of the enantiomeric pure suspension would be mixed with the racemic suspension before entering the reactor. Another possibility would be the use of chiral additives [60], with the drawback that these additives might have to be separated again after the deracemization process.

Last but not least, it could be possible to optimize the deracemization by combining the resolution via temperature cycles with attrition enhanced ripening. This could be achieved for example via applying ultrasonic waves to the cold water bath, where the growth of the crystals takes place. Using this setup, the crystal sizes would be small during the whole experiments, which accelerates the process [7].

6 Summary

Enantiomeric purity is very important for many chemical compounds, as enantiomers react differently in a chiral environment [14]. Especially for active pharmaceutical components and when only one enantiomer is helpful for the human body, care has to be taken of a high enantiomeric purity [2]. Resolution can be achieved via several methods, but temperature cycling is particularly promising, since complete deracemization can be achieved in one step [8].

In this master's thesis, a crystallization setup including temperature cycling was investigated. For this purpose, crystals with an initial enantioimbalance of about 5 % were cycled in their respective saturated solution through a tubular reactor trough a colder and a warmer water bath, compared to ambient temperature. The reactor diameter was 2 mm, the total length 48 m and 12 cycles were used. To avoid sedimentation, air was added via a syringe pump to generate a slug flow profile. The used model system consisted of *N*-(2-methylbenzylidene)-phenylglycine amide (NMPA), ethanol and the catalyst 1,8-diazabicyclo[5.4.0]undec-7-ene. At the end of each experiment the crystals were filtered and washed with cold water to remove the solvent and the catalyst.

It was possible to achieve an increase of the enantiomeric excess during cycling through water baths. The experiments were most reproducible with small particle sizes. Furthermore, the influence of the water bath temperatures, amount of catalyst, pump rate and crystal mass were investigated. To make a comparison of the experiments possible and to get a value of how advanced the deracemization was, the cycle number based deracemization constant k_N and the productivity P were used. An increase of the water bath temperature difference resulted in a faster deracemization and a higher productivity until excessively high differences induced nucleation. Both values were also improved via a high catalyst amount, whereby no limit was detected yet. Contrary, a higher pump rate or crystal mass slowed down the deracemization, whereby the productivity increased. Deracemization with the fastest process conditions with a pump rate of 10 mL/min and a k_N of 0.097 would require only 22.62 min in 18 cycles. This results in a reactor volume of 0.905 l and a time of 1 h and 40 min for total resolution of 1 L suspension.

It was also successfully proven that it is possible to extend the residence time while pumping the suspension several times through the reactor, when the end of the tube is fixed to the beginning. For this, saturated solution had to be added via a syringe to avoid degassing due to pressure loss resulting from diffusion of ethanol through the tube. Overall, it could be shown that applying temperature cycles to a suspension in continuous flow is a promising approach for deracemization of chiral compounds.

7 Appendix

7.1 Used chemicals

The chemicals were purchased from the providers in table 7.1 and used without further treatment.

Table 7.1: Purchased chemicals

Substance	Purity	Provider
methanol	99 %	Carl Roth
iso-propanol	99.8 %	Chem Lab
n-hexane	99 %	Chem Lab
2-phenylglycine	95 %	Sigma Aldrich
o-tolualdehyde	96.5 %	Sigma Aldrich
ammonium hydroxide	33 %	J. T. Baker
acetonitrile	99.9 %	Chem Lab
thionyl chloride	99 %	Fluka
1,8-diazabicyclo[5.4.0]undec-7-ene	98 %	Sigma Aldrich
ethanol	99.8 %	Carl Roth

7.2 Substance properties

NMPA: molar mass: 252.31 g/mol, calculated with ChemSketch®
DBU: molar mass: 152.24 g/mol, density: 1.02 g/mL at 20 °C [78]
Ethanol: molar mass: 46.07 g/mol, density: 0.789 g/mL at 20 °C [79]

7.3 Solubility data

The data of the solubility measurements S1-S12 with a maximum temperature of 70 °C and a stirring rate of 600 rpm can be taken from table 7.2. From table 7.3, the data of the experiments S13-S15 can be taken, which show the influence of the maximum temperature and stirring speed. Finally, the data of the experiments S16-S29 with varying maximum temperatures can be taken from table 7.4. All measurements were performed with a Crystalline® device.

Table 7.2: Concentration dependent dissolving temperature of NMPA in ethanol, estimated by a Crystalline® device in several cylces, maximum temperature: 70 °C, minimum temperature: -10 °C, heating and cooling rates: 0.5 °C/min, stirring rate: 600 rpm.

notation	ethanol [g]	NMPA [g]	c [mg/g]	T_1 [°C]	T_2 [°C]	T_3 [°C]
S1	2.9995	0.1704	56.8095	56.8	53.9	51.1
S2	3.0034	0.1500	49.9434	55.3	52.5	49.9
S3	3.0034	0.1305	43.4508	53.1	49.2	45.8
S4	3.0000	0.1100	36.6667	48.3	44.4	41.1
S5	3.0041	0.0900	29.9591	44.9	41.0	38.3
S6	3.0029	0.0702	23.3774	39.3	35.4	32.8
S7	2.9970	0.0700	23.3567	39.7	36.7	33.6
S8	3.0116	0.0503	16.7021	32.6	24.5	19.5
S9	3.0000	0.0500	16.6667	31.7	27.2	24.6
S10	3.0038	0.0500	16.6456	33.3	30.1	27.6
S11	2.9967	0.0304	10.1445	22.0	19.2	16.5
S12	3.0014	0.0202	6.7302	10.2	7.8	-

Table 7.3: Concentration dependent dissolving temperature of NMPA in ethanol, estimated by a Crystalline® device in several cylces, minimum temperature: -10 °C, heating and cooling rates: 0.5 °C/min, influence of maximum temperature T_{max} and stirring rate U.

notation	ethanol [g]	NMPA [g]	c [mg/g]	U [rpm]	T_{max} [°C]	T_1 [°C]	T_2 [°C]	T_3 [°C]
S13	3.0000	0.0302	10.0667	600	70.0	21.6	18	14.9
S14	3.0000	0.0300	10.0000	600	50.0	20.8	19.4	19
S15	3.0000	0.0300	10.0000	400	50.0	21.3	20.3	19.6

Table 7.4: Concentration dependent dissolving temperature of NMPA in ethanol, estimated by a Crystalline® device in several cylces, for different maximum temperatures, minimum temperature: -10 °C, heating and cooling rates: 0.5 °C/min, stirring rate: 500 rpm.

notation	ethanol [g]	NMPA [g]	c [mg/g]	T_{max} [°C]	T_1 [°C]	T_2 [°C]	T_3 [°C]	T_4 [°C]
S16	3.0154	0.0907	30.0789	45.0	45.0	44.9	44.7	44.4
S17	3.0087	0.0796	26.4566	45.0	42.1	42.0	41.4	41.0
S18	3.0222	0.0696	23.0296	45.0	38.0	38.8	38.4	37.9
S19	3.0114	0.0689	22.8797	40.0	38.7	38.4	38.3	-
S20	3.0029	0.0597	19.8808	40.0	35.1	34.6	34.7	-
S21	3.0020	0.0498	16.5889	35.0	31.9	31.9	32.0	32.0
S22	3.0000	0.0399	13.3000	30.0	27.9	27.1	27.3	27.1
S23	3.0069	0.0350	11.6399	25.0	23.7	23.5	23.4	23.3
S24	3.0039	0.0302	10.0536	25.0	21.0	19.5	20.2	-
S25	3.0389	0.0305	10.0365	25.0	21.5	20.7	20.8	-
S26	3.0036	0.0254	8.4565	25.0	20.3	17.9	17.6	17.5
S27	3.0123	0.0246	8.1665	20.0	15.9	16.4	15.8	-
S28	3.0052	0.0212	7.0544	15.0	15.0	13.1	13.1	-
S29	3.0081	0.0172	5.7179	25.0	10.1	9.9	-	-

7.4 Experimental data

The data of the continuous deracemization experiments E1-E50 in a tubular reactor can be taken from tables 7.5, 7.6, 7.7, 7.8 and 7.9. Care has to be taken that at the experiments E1-E8, E11, E12, E17 and E18 the suspension at the beginning was not discarded for exactly 1.5 min.

Table 7.5: Initial enantiomeric excess of the suspension after 5 min and 15 min mixing, as well as the mean of them, experimentally obtained enantiomeric excess and cycle number based deracemization constant for NMPA in ethanol in a 48 m tubular reactor, coiled up in 12 cycles, water bath temperature difference: 10 °C, 5 µL/g_{total} DBU, fluid pump rate: 4 mL/min, ratio air/fluid: 0.2, dry crystal mass: 0.3 wt%, influence of grinding, E: enantiomerically enriched crystals, R: racemic crystals.

notation	$ee_{0,5\,\mathrm{min}}$ [%]	$ee_{0,15\,\mathrm{min}}$ [%]	$ee_{0,\mathrm{mean}}$ [%]	ee [%]	k_N	specification
E1	12.388	6.366	9.377	31.388	0.101	E and R not ground
E2	11.526	16.000	13.763	31.578	0.069	E and R not ground
E3	12.688	12.012	12.350	38.944	0.096	R are ground
E4	10.398	16.224	13.311	18.224	0.026	R are ground
E5	10.862	15.274	13.068	39.800	0.093	E and R are ground
E6	12.138	15.148	13.643	35.834	0.080	E and R are ground
E7	11.112	10.682	10.897	32.498	0.091	R are ground
E8	8.692	8.992	8.842	27.086	0.093	R are ground

Table 7.6: Initial enantiomeric excess of the suspension after 5 min and 15 min mixing, as well as the mean of them, experimentally obtained enantiomeric excess and cycle number based deracemization constant for NMPA in ethanol at various water bath temperature differences, in a 48 m tubular reactor, coiled up in 12 cycles, 5 $\mu L/g_{total}$ DBU, fluid pump rate: 4 mL/min, ratio air/fluid: 0.2, dry crystal mass: 0.3 wt%.

notation	ΔT [°C]	$ee_{0,5\,min}$ [%]	$ee_{0,15\,min}$ [%]	$ee_{0,mean}$ [%]	ee [%]	k_N	$k_{N,mean}$
E9	2	2.294	7.382	4.838	7.228	0.033	
E10	2	3.654	4.244	3.949	6.198	0.038	0.036
E11	4	4.872	4.548	4.710	10.550	0.067	
E12	4	6.458	7.422	6.940	10.916	0.038	0.052
E13	6	3.158	3.682	3.420	8.368	0.075	
E14	6	5.200	4.152	4.676	11.514	0.075	0.075
E15	8	4.054	3.550	3.802	9.346	0.075	
E16	8	2.778	3.156	2.967	10.184	0.103	0.089
E17	10	6.232	7.584	6.908	29.948	0.122	
E18	10	7.276	7.420	7.348	27.108	0.109	0.116
E19	12	3.282	4.628	3.955	19.622	0.133	
E20	12	3.726	3.924	3.825	24.058	0.153	0.143
E21	24	2.214	2.104	2.159	17.236	0.173	
E22	24	2.714	2.886	2.800	13.706	0.132	0.153
E23	29	4.398	6.146	5.272	14.860	0.086	
E24	29	8.454	7.320	7.887	17.070	0.064	0.075

Table 7.7: Initial enantiomeric excess of the suspension after 5 min and 15 min mixing, as well as the mean of them, experimentally obtained enantiomeric excess and cycle number based deracemization constant for NMPA in ethanol for various catalyst amounts in a 48 m tubular reactor, coiled up in 12 cycles, water bath temperature difference: 10 °C, fluid pump rate: 4 mL/min, ratio air/fluid: 0.2, dry crystal mass: 0.3 wt%.

notation	DBU [$\mu L/g_{total}$]	$ee_{0,5\,min}$ [%]	$ee_{0,15\,min}$ [%]	$ee_{0,mean}$ [%]	ee [%]	k_N	$k_{N,mean}$
E25	7	3.632	3.472	3.552	27.992	0.172	
E26	7	3.260	3.396	3.328	14.292	0.121	0.147
E27	6	3.346	5.038	4.192	27.658	0.157	
E28	6	4.294	3.852	4.073	14.230	0.104	0.131
E29	5	6.232	7.584	6.908	29.948	0.122	
E30	5	7.276	7.420	7.348	27.108	0.109	0.116
E31	3	6.276	5.412	5.844	18.426	0.096	
E32	3	2.164	3.936	3.050	10.108	0.100	0.098
E33	1	3.508	6.570	5.039	11.486	0.069	
E34	1	5.058	8.748	6.903	27.254	0.114	0.092

Table 7.8: Initial enantiomeric excess of the suspension after 5 min and 15 min mixing, as well as the mean of them, experimentally obtained enantiomeric excess and cycle number based deracemization constant for NMPA in ethanol for various fluid pump rates in a 48 m tubular reactor, coiled up in 12 cycles, water bath temperature difference: 10 °C, 5 $\mu L/g_{total}$ DBU, ratio air/fluid: 0.2, dry crystal mass: 0.3 wt%.

notation	F_V [mL/min]	$ee_{0,5\,min}$ [%]	$ee_{0,15\,min}$ [%]	$ee_{0,mean}$ [%]	ee [%]	k_N	$k_{N,mean}$
E35	10	3.450	4.312	3.881	11.920	0.094	
E36	10	2.690	6.494	4.592	15.352	0.101	0.097
E37	6	7.984	5.542	6.763	25.954	0.112	
E38	6	4.626	8.246	6.436	22.448	0.104	0.108
E39	5	7.102	5.928	6.515	29.466	0.126	
E40	5	5.642	7.024	6.333	19.418	0.093	0.110
E41	4	6.232	7.584	6.908	29.948	0.122	
E42	4	7.276	7.420	7.348	27.108	0.109	0.116

Table 7.9: Initial enantiomeric excess of the suspension after 5 min and 15 min mixing, as well as the mean of them, experimentally obtained enantiomeric excess and cycle number based deracemization constant for NMPA in ethanol for various dry crystal masses in a 48 m tubular reactor, coiled up in 12 cycles, water bath temperature difference: 10 °C, 5 $\mu L/g_{total}$ DBU, fluid pump rate: 4 mL/min, ratio air/fluid: 0.2.

notation	DBU [$\mu L/g_{total}$]	$ee_{0,5\,min}$ [%]	$ee_{0,15\,min}$ [%]	$ee_{0,mean}$ [%]	ee [%]	k_N	$k_{N,mean}$
E43	1	3.938	4.130	4.034	7.370	0.050	
E44	1	4.446	6.038	5.242	9.372	0.048	0.049
E45	0.8	4.054	4.240	4.147	9.074	0.065	
E46	0.8	4.016	4.908	4.462	8.118	0.050	0.058
E47	0.5	3.542	4.076	3.809	10.186	0.082	
E48	0.5	3.426	4.644	4.035	11.406	0.087	0.084
E49	0.3	6.232	7.584	6.908	29.948	0.122	
E50	0.3	7.276	7.420	7.348	27.108	0.109	0.116

7.5 Calculation of the productivity

The calculated productivities as well as the cycle number based deracemization constants and the required times and cycles to reach complete deracemization of the experiments E1-E50 are summarized in tables 7.10, 7.11, 7.12 and 7.13. All calculations were performed with a cycle volume of 0.0126 L, a suspension mass of 80 g, 0.3 wt% solid crystal mass and a pump rate of 4 ml/min, if not declared otherwise.

Table 7.10: Calculated required amount of cycles, calculated total process time and calculated productivity for the deracemization of NMPA in ethanol with an ee_0 of 18 % for various water bath temperatures, the calculations were performed with the cycle number based deracemization constants observed in a 48 m tubular reactor, coiled up in 12 cycles, 5 µL/g_{total} DBU, fluid pump rate: 4 mL/min, ratio air/fluid: 0.2, dry crystal mass: 0.3 wt%, mean value of two experiments

Δ T [°C]	k_N	cycles	t [h]	P [kg/(m^3·h)]
2	0.036	49	153.94	0.378
4	0.052	33	103.67	0.562
6	0.075	23	72.26	0.806
8	0.089	20	62.83	0.927
10	0.116	15	47.12	1.236
12	0.143	12	37.70	1.545
24	0.153	12	37.70	1.545
29	0.075	23	72.26	0.806

Table 7.11: Calculated required amount of cycles, calculated total process time and calculated productivity for the deracemization of NMPA in ethanol with an ee_0 of 18 % for various amounts of DBU, the calculations were performed with the cycle number based deracemization constants observed in a 48 m tubular reactor, coiled up in 12 cycles, water bath temperature difference: 10 °C, fluid pump rate: 4 mL/min, ratio air/fluid: 0.2, dry crystal mass: 0.3 wt%, mean value of two experiments

DBU [µL/g_{total}]	k_N	cycles	t [h]	P [kg/(m^3·h)]
1	0.092	19	59.69	0.976
3	0.098	18	56.55	1.030
5	0.116	15	47.12	1.236
6	0.131	14	43.98	1.324
7	0.147	12	37.70	1.545

Table 7.12: Calculated required amount of cycles, calculated time per cycle, calculated total process time and calculated productivity for the deracemization of NMPA in ethanol with an ee_0 of 18 % for various pump rates, the calculations were performed with the cycle number based deracemization constants observed in a 48 m tubular reactor, coiled up in 12 cycles, water bath temperature difference: 10 °C, 5 µL/g_{total} DBU, ratio air/fluid: 0.2, dry crystal mass: 0.3 wt%, mean value of two experiments

F_V [mL/min]	t_{cycle}	k_N	cycles	t [h]	P [kg/(m^3·h)]
4	3.14	0.116	15	47.12	1.236
5	2.51	0.110	16	40.21	1.448
6	2.09	0.108	16	33.51	1.738
10	1.26	0.097	18	22.62	2.574

Table 7.13: Calculated required amount of cycles, calculated total process time and calculated productivity for the deracemization of NMPA in ethanol with an ee_0 of 18 % for various dry crystal masses, the calculations were performed with the cycle number based deracemization constants observed in a 48 m tubular reactor, coiled up in 12 cycles, water bath temperature difference: 10 °C, 5 µL/g_{total} DBU, fluid pump rate: 4 mL/min, ratio air/fluid: 0.2, mean value of two experiments

Δ T [°C]	k_N	cycles	t [h]	P [kg/(m³·h)]	
0.3	0.24	0.116	15	47.12	1.236
0.5	0.4	0.084	21	65.97	1.471
0.8	0.64	0.058	30	94.25	1.648
1	0.8	0.049	35	109.96	1.765

8 Symbol register

T	°C	temperature
R	g	mass of R enantiomer
S	g	mass of S enantiomer
ee	-	enantiomeric excess
t	min	time
N	-	number of cycles
k	1/min	temperature based deracemization constant
k_N	-	cycle number based deracemization constant
c	mg/g	concentration
V	L	reactor volume
F	moles/min	molar flow
F_V	mL/min	volumetric flow
r	moles/(l·min)	reaction rate
X	-	conversion
$\dot{Q}$	J	heat
$\dot{W}_s$	J	shaft therm
cp	J/(moles·K)	molar heat capacity
Δcp	J/(moles·K)	change of the heat capacity per mole of A reacted
Θ	-	ratio of number of moles to A
$\Delta H_R(T)$	J/mol	heat of reaction at temperature T per mole of A
$\Delta H_R^\circ(T_R)$	J/mol	heat of reaction at the reference temperature T_R per mole of A
Z	-	location of cross section
U	rpm	stirring rate
ρ	g/mL	density

8.1 Indices

i	species
A	limiting species
0	entering the reactor
R	reference state

Bibliography

[1] Izake, Emad L.: Chiral discrimination and enantioselective analysis of drugs: an overview. In: *Journal of pharmaceutical sciences* 96 (2007), Nr. 7, S. 1659–1676. http://dx.doi.org/10.1002/jps.20820. – DOI 10.1002/jps.20820. – ISSN 0022–3549

[2] Agranat, Israel ; Caner, Hava ; Caldwell, John: Putting chirality to work: the strategy of chiral switches. In: *Nature reviews. Drug discovery* 1 (2002), Nr. 10, S. 753–768. http://dx.doi.org/10.1038/nrd915. – DOI 10.1038/nrd915. – ISSN 1474–1776

[3] Clayden, Jonathan ; Greeves, Nick ; Warren, Stuart G.: *Organische Chemie.* 2. Auflage [=1. deutsche Ausgabe]. Berlin and Heidelberg : Springer Spektrum, 2013 (Lehrbuch). http://www.springer.com/de/book/9783642347153. – ISBN 9783642347153

[4] Lorenz, Heike ; Seidel-Morgenstern, Andreas: Processes to separate enantiomers. In: *Angewandte Chemie (International ed. in English)* 53 (2014), Nr. 5, S. 1218–1250. http://dx.doi.org/10.1002/anie.201302823. – DOI 10.1002/anie.201302823

[5] Kaspereit, Malte ; García Palacios, Javier ; Meixús Fernández, Tania ; Kienle, Achim: *Computer Aided Chemical Engineering.* Bd. 25: *Systematic design of production processes for enantiomers with integration of chromatography and racemisation reactions.* 2008. http://dx.doi.org/10.1016/S1570-7946(08)80021-1. http://dx.doi.org/10.1016/S1570-7946(08)80021-1. – ISBN 9780444532275

[6] Viedma, Cristobal: Chiral symmetry breaking during crystallization: complete chiral purity induced by nonlinear autocatalysis and recycling. In: *Physical review letters* 94 (2005), Nr. 6, S. 065504. http://dx.doi.org/10.1103/PhysRevLett.94.065504. – DOI 10.1103/PhysRevLett.94.065504. – ISSN 0031–9007

[7] Noorduin, Wim L. ; Izumi, Toshiko ; Millemaggi, Alessia ; Leeman, Michel ; Meekes, Hugo ; van Enckevort, Willem J. P. ; Kellogg, Richard M. ; Kaptein, Bernard ; Vlieg, Elias ; Blackmond, Donna G.: Emergence of a single solid chiral state from a nearly racemic amino acid derivative. In: *Journal of the American Chemical Society* 130 (2008), Nr. 4, S. 1158–1159. http://dx.doi.org/10.1021/ja7106349. – DOI 10.1021/ja7106349

[8] Suwannasang, K. ; Flood, A. E. ; Rougeot, C. ; Coquerel, G.: Using Programmed Heating–Cooling Cycles with Racemization in Solution for Complete Symmetry Breaking of a Conglomerate Forming System. In: *Crystal growth & design*

13 (2013), Nr. 8, S. 3498–3504. http://dx.doi.org/10.1021/cg400436r. – DOI 10.1021/cg400436r. – ISSN 1528–7483

[9] Eder, Rafael J. P. ; Schrank, Simone ; Besenhard, Maximilian O. ; Roblegg, Eva ; Gruber-Woelfler, Heidrun ; Khinast, Johannes G.: Continuous Sonocrystallization of Acetylsalicylic Acid (ASA): Control of Crystal Size. In: *Crystal growth & design* 12 (2012), Nr. 10, S. 4733–4738. http://dx.doi.org/10.1021/cg201567y. – DOI 10.1021/cg201567y. – ISSN 1528–7483

[10] Eder, R. J. P. ; Schmitt, E. K. ; Grill, J. ; Radl, S. ; Gruber-Woelfler, H. ; Khinast, J. G.: Seed loading effects on the mean crystal size of acetylsalicylic acid in a continuous-flow crystallization device. In: *Crystal Research and Technology* 46 (2011), Nr. 3, S. 227–237. http://dx.doi.org/10.1002/crat.201000634. – DOI 10.1002/crat.201000634. – ISSN 02321300

[11] Pérez-Calvo, José-Francisco ; Kadam, Somnath S. ; Kramer, Herman J. M.: Determination of kinetics in batch cooling crystallization processes-A sequential parameter estimation approach. In: *AIChE Journal* 62 (2016), Nr. 11, S. 3992–4012. http://dx.doi.org/10.1002/aic.15295. – DOI 10.1002/aic.15295. – ISSN 00011541

[12] Besenhard, Maximilian O. ; Neugebauer, Peter ; Scheibelhofer, Otto ; Khinast, Johannes G.: Crystal Engineering in Continuous Plug-Flow Crystallizers. In: *Crystal growth & design* 17 (2017), Nr. 12, S. 6432–6444. http://dx.doi.org/10.1021/acs.cgd.7b01096. – DOI 10.1021/acs.cgd.7b01096. – ISSN 1528–7483

[13] Robert J. Ouellette ; J. David Rawn: 6 - Stereochemistry. Version: 2015. http://dx.doi.org/10.1016/B978-0-12-802444-7.00006-9. In: Ouellette, Robert J. (Hrsg.) ; Rawn, J. D. (Hrsg.): *Principles of Organic Chemistry*. Boston : Elsevier, 2015. – DOI 10.1016/B978–0–12–802444–7.00006–9. – ISBN 978–0–12–802444–7, 163–188

[14] Scriba, Gerhard K. E.: Recognition Mechanisms of Chiral Selectors: An Overview. In: *Methods in molecular biology (Clifton, N.J.)* 1985 (2019), S. 1–33. http://dx.doi.org/10.1007/978-1-4939-9438-0{_}1. – DOI 10.1007/978–1–4939–9438–0_1

[15] Nafie, Laurence A. ; Dukor, Rina K.: Chapter 5 - Vibrational Optical Activity in Chiral Analysis. Version: 2018. http://dx.doi.org/10.1016/B978-0-444-64027-7.00005-7. In: Prasad L. Polavarapu (Hrsg.): *Chiral Analysis (Second Edition)*. Elsevier, 2018. – DOI 10.1016/B978–0–444–64027–7.00005–7. – ISBN 978–0–444–64027–7, 201–247

[16] Rougeot, Céline ; Hein, Jason E.: Application of Continuous Preferential Crystallization to Efficiently Access Enantiopure Chemicals. In: *Organic Process Research & Development* 19 (2015), Nr. 12, S. 1809–1819. http://dx.doi.org/10.1021/acs.oprd.5b00141. – DOI 10.1021/acs.oprd.5b00141. – ISSN 1083–6160

[17] Marckwald, W. ; Kenzie, Alex. M.: Ueber eine principiell neue Methode zur Spaltung racemischer Verbindungen in die activen Bestandtheile. In: *Berichte der deutschen chemischen Gesellschaft* 32 (1899), Nr. 2, S. 2130–2136. http://dx.doi.org/10.1002/cber.189903202130. – DOI 10.1002/cber.189903202130. – ISSN 03659496

[18] Breuer, Michael ; Ditrich, Klaus ; Habicher, Tilo ; Hauer, Bernhard ; Kesseler, Maria ; Stürmer, Rainer ; Zelinski, Thomas: Industrial methods for the production of optically active intermediates. In: *Angewandte Chemie (International ed. in English)* 43 (2004), Nr. 7, S. 788–824. http://dx.doi.org/10.1002/anie.200300599. – DOI 10.1002/anie.200300599

[19] Fogassy, Elemér ; Nógrádi, Mihály ; Kozma, Dávid ; Egri, Gabriella ; Pálovics, Emese ; Kiss, Violetta: Optical resolution methods. In: *Organic & biomolecular chemistry* 4 (2006), Nr. 16, S. 3011–3030. http://dx.doi.org/10.1039/b603058k. – DOI 10.1039/b603058k. – ISSN 1477–0520

[20] Li, Wei W. ; Spix, Laura ; Reus, Saskia C. A. ; Meekes, Hugo ; Kramer, Herman J. M. ; Vlieg, Elias ; Ter Horst, Joop H.: Deracemization of a Racemic Compound via Its Conglomerate-Forming Salt Using Temperature Cycling. In: *Crystal growth & design* 16 (2016), Nr. 9, S. 5563–5570. http://dx.doi.org/10.1021/acs.cgd.6b01034. – DOI 10.1021/acs.cgd.6b01034. – ISSN 1528–7483

[21] Rougeot, Céline ; Guillen, Frédéric ; Plaquevent, Jean-Christophe ; Coquerel, Gérard: Ultrasound-Enhanced Deracemization: Toward the Existence of Agonist Effects in the Interpretation of Spontaneous Symmetry Breaking. In: *Crystal growth & design* 15 (2015), Nr. 5, S. 2151–2155. http://dx.doi.org/10.1021/cg501765g. – DOI 10.1021/cg501765g. – ISSN 1528–7483

[22] Xiouras, Christos ; van Aeken, Jasper ; Panis, Joris ; Ter Horst, Joop H. ; van Gerven, Tom ; Stefanidis, Georgios D.: Attrition-Enhanced Deracemization of NaClO 3 : Comparison between Ultrasonic and Abrasive Grinding. In: *Crystal growth & design* 15 (2015), Nr. 11, S. 5476–5484. http://dx.doi.org/10.1021/acs.cgd.5b01108. – DOI 10.1021/acs.cgd.5b01108. – ISSN 1528–7483

[23] Ruecroft, Graham ; Hipkiss, David ; Ly, Tuan ; Maxted, Neil ; Cains, Peter W.: Sonocrystallization: The Use of Ultrasound for Improved Industrial Crystallization. In: *Organic Process Research & Development* 9 (2005), Nr. 6, S. 923–932. http://dx.doi.org/10.1021/op050109x. – DOI 10.1021/op050109x. – ISSN 1083–6160

[24] Suwannasang, Kittisak ; Flood, Adrian E. ; Coquerel, Gérard: A Novel Design Approach To Scale Up the Temperature Cycle Enhanced Deracemization Process: Coupled Mixed-Suspension Vessels. In: *Crystal growth & design* 16 (2016), Nr. 11, S. 6461–6467. http://dx.doi.org/10.1021/acs.cgd.6b01139. – DOI 10.1021/acs.cgd.6b01139. – ISSN 1528–7483

[25] Eder, Rafael J. P. ; Radl, Stefan ; Schmitt, Elisabeth ; Innerhofer, Sabine ; Maier, Markus ; Gruber-Woelfler, Heidrun ; Khinast, Johannes G.: Continuously Seeded, Continuously Operated Tubular Crystallizer for the Production of Active Pharmaceutical Ingredients. In: *Crystal growth & design* 10 (2010), Nr. 5, S. 2247–2257. http://dx.doi.org/10.1021/cg9015788. – DOI 10.1021/cg9015788. – ISSN 1528–7483

[26] Variankaval, Narayan ; Cote, Aaron S. ; Doherty, Michael F.: From form to function: Crystallization of active pharmaceutical ingredients. In: *AIChE Journal* 54 (2008), Nr. 7, S. 1682–1688. http://dx.doi.org/10.1002/aic.11555. – DOI 10.1002/aic.11555. – ISSN 00011541

[27] Gros, Håkan ; Kilpiö, Teuvo ; Nurmi, Juha: Continuous cooling crystallization from solution. In: *Powder Technology* 121 (2001), Nr. 1, S. 106–115. http://dx.doi.org/10.1016/S0032-5910(01)00382-5. – DOI 10.1016/S0032–5910(01)00382–5. – ISSN 00325910

[28] Laurence A. Nafie ; Rina K. Dukor: Chapter 5 - Vibrational Optical Activity in Chiral Analysis. Version: 2018. http://dx.doi.org/10.1016/B978-0-444-64027-7.00005-7. In: Prasad L. Polavarapu (Hrsg.): *Chiral Analysis (Second Edition)*. Elsevier, 2018. – DOI 10.1016/B978–0–444–64027–7.00005–7. – ISBN 978–0–444–64027–7, 201–247

[29] Steendam, René R. E. ; Harmsen, Bram ; Meekes, Hugo ; van Enckevort, Willem J. P. ; Kaptein, Bernard ; Kellogg, Richard M. ; Raap, Jan ; Rutjes, Floris P. J. T. ; Vlieg, Elias: Controlling the Effect of Chiral Impurities on Viedma Ripening. In: *Crystal growth & design* 13 (2013), Nr. 11, S. 4776–4780. http://dx.doi.org/10.1021/cg400927m. – DOI 10.1021/cg400927m. – ISSN 1528–7483

[30] Beckmann, Wolfgang: Crystallization: Introduction. Version: 2013. http://dx.doi.org/10.1002/9783527650323.ch1. In: Beckmann, Wolfgang (Hrsg.): *Crystallization*. Weinheim : Wiley-VCH, 2013. – DOI 10.1002/9783527650323.ch1. – ISBN 9783527650323, S. 1–5

[31] Lorenz, Heike: Solubility and Solution Equilibria in Crystallization. Version: 2013. http://dx.doi.org/10.1002/9783527650323.ch3. In: Beckmann, Wolfgang (Hrsg.): *Crystallization* Bd. 10. Weinheim : Wiley-VCH, 2013. – DOI 10.1002/9783527650323.ch3. – ISBN 9783527650323, S. 35–74

[32] Beckmann, Wolfgang: Mechanisms of Crystallization. Version: 2013. http://dx.doi.org/10.1002/9783527650323.ch2. In: Beckmann, Wolfgang (Hrsg.): *Crystallization*. Weinheim : Wiley-VCH, 2013. – DOI 10.1002/9783527650323.ch2. – ISBN 9783527650323, S. 7–33

[33] Wieckhusen, Dierk: Development of Batch Crystallizations. Version: 2013. http://dx.doi.org/10.1002/9783527650323.ch10. In: Beckmann, Wolfgang (Hrsg.):

Crystallization. Weinheim : Wiley-VCH, 2013. – DOI 10.1002/9783527650323.ch10. – ISBN 9783527650323, S. 187–202

[34] Beckmann, Wolfgang: Basics of Industrial Crystallization from Solution. Version: 2013. http://dx.doi.org/10.1002/9783527650323.ch9. In: Beckmann, Wolfgang (Hrsg.): *Crystallization*. Weinheim : Wiley-VCH, 2013. – DOI 10.1002/9783527650323.ch9. – ISBN 9783527650323, S. 173–185

[35] Wieckhusen, Dierk: Development of Batch Crystallizations: 10. Version: 2013. http://dx.doi.org/10.1002/9783527650323.ch10. In: *Crystallization*. John Wiley & Sons, Ltd, 2013. – DOI 10.1002/9783527650323.ch10. – ISBN 9783527650323, S. 187–202

[36] Hellwich, Karl-Heinz: *Stereochemie: Grundbegriffe*. 2., erw. Aufl. Berlin : Springer, 2007 http://deposit.d-nb.de/cgi-bin/dokserv?id=2971846&prov=M&dok_var=1&dok_ext=htm. – ISBN 9783540717072

[37] Kondepudi, Dilip: Chapter 1 - Chiral Asymmetry in Nature. Version: 2018. http://dx.doi.org/10.1016/B978-0-444-64027-7.00001-X. In: Prasad L. Polavarapu (Hrsg.): *Chiral Analysis (Second Edition)*. Elsevier, 2018. – DOI 10.1016/B978–0–444–64027–7.00001–X. – ISBN 978–0–444–64027–7, 3–28

[38] Holm, Nils G.: Chapter 1 Why are hydrothermal systems proposed as plausible environments for the origin of life? In: *Origins of Life and Evolution of the Biosphere* 22 (1992), Nr. 1-4, S. 5–14. http://dx.doi.org/10.1007/BF01808015. – DOI 10.1007/BF01808015. – ISSN 0169–6149

[39] Busch, Kenneth W. ; Busch, Marianna A.: Chapter 3 - Light Polarization and Signal Processing in Chiroptical Instrumentation. Version: 2018. http://dx.doi.org/10.1016/B978-0-444-64027-7.00003-3. In: Prasad L. Polavarapu (Hrsg.): *Chiral Analysis (Second Edition)*. Elsevier, 2018. – DOI 10.1016/B978–0–444–64027–7.00003–3. – ISBN 978–0–444–64027–7, 73–151

[40] Kuwahara, Shunsuke ; Ikeda, Mari ; Habata, Yoichi: Chapter 8 - Chiroptical Probes for Determination of Absolute Stereochemistry by Circular Dichroism Exciton Chirality Method. Version: 2018. http://dx.doi.org/10.1016/B978-0-444-64027-7.00008-2. In: Prasad L. Polavarapu (Hrsg.): *Chiral Analysis (Second Edition)*. Elsevier, 2018. – DOI 10.1016/B978–0–444–64027–7.00008–2. – ISBN 978–0–444–64027–7, 345–366

[41] Balzano, Federica ; Uccello-Barretta, Gloria ; Aiello, Federica: Chapter 9 - Chiral Analysis by NMR Spectroscopy: Chiral Solvating Agents. Version: 2018. http://dx.doi.org/10.1016/B978-0-444-64027-7.00009-4. In: Prasad L. Polavarapu (Hrsg.): *Chiral Analysis (Second Edition)*. Elsevier, 2018. – DOI 10.1016/B978–0–444–64027–7.00009–4. – ISBN 978–0–444–64027–7, 367–427

[42] Havinga, E.: Spontaneous formation of optically active substances. In: *Biochimica et Biophysica Acta* 13 (1954), S. 171–174. http://dx.doi.org/10.1016/0006-3002(54)90300-5. – DOI 10.1016/0006–3002(54)90300–5. – ISSN 00063002

[43] Suwannasang, Kittisak ; Flood, Adrian E. ; Rougeot, Celine ; Coquerel, Gerard: Use of Programmed Damped Temperature Cycles for the Deracemization of a Racemic Suspension of a Conglomerate Forming System. In: *Organic Process Research & Development* 21 (2017), Nr. 4, S. 623–630. http://dx.doi.org/10.1021/acs.oprd.7b00028. – DOI 10.1021/acs.oprd.7b00028. – ISSN 1083–6160

[44] Jacques, Jean ; Collet, André ; Wilen, Samuel H.: *Enantiomers, racemates, and resolutions*. Reissue with corr. Malabar, Fl. : Krieger, 1994. – ISBN 0894648764

[45] Srisanga, Sukanya ; Ter Horst, Joop H.: Racemic Compound, Conglomerate, or Solid Solution: Phase Diagram Screening of Chiral Compounds. In: *Crystal growth & design* 10 (2010), Nr. 4, S. 1808–1812. http://dx.doi.org/10.1021/cg901483v. – DOI 10.1021/cg901483v. – ISSN 1528–7483

[46] Spix, Laura ; Alfring, Alinda ; Meekes, Hugo ; van Enckevort, Willem J. P. ; Vlieg, Elias: Formation of a Salt Enables Complete Deracemization of a Racemic Compound through Viedma Ripening. In: *Crystal growth & design* 14 (2014), Nr. 4, S. 1744–1748. http://dx.doi.org/10.1021/cg4018882. – DOI 10.1021/cg4018882. – ISSN 1528–7483

[47] Kimoto, Hiroki ; Saigo, Kazuhiko ; Ohashi, Yuji ; Hasegawa, Masaki: Molecular Recognition in the Formation of Conglomerate Crystal. 2. The Role of Arenesulfonic Acid in the Conglomerate Crystals of Amino Acid Salts. In: *Bulletin of the Chemical Society of Japan* 62 (1989), Nr. 7, S. 2189–2195. http://dx.doi.org/10.1246/bcsj.62.2189. – DOI 10.1246/bcsj.62.2189. – ISSN 0009–2673

[48] Iggland, Martin ; Mazzotti, Marco: A Population Balance Model for Chiral Resolution via Viedma Ripening. In: *Crystal growth & design* 11 (2011), Nr. 10, S. 4611–4622. http://dx.doi.org/10.1021/cg2008599. – DOI 10.1021/cg2008599. – ISSN 1528–7483

[49] Mersmann, A.: Crystallization Technology Handbook. In: *Drying Technology* 13 (1995), Nr. 4, S. 1037–1038. http://dx.doi.org/10.1080/07373939508917003. – DOI 10.1080/07373939508917003. – ISSN 0737–3937

[50] Ståhl, Marie ; Åslund, Bengt ; Rasmuson, Åke C.: Aging of Reaction-Crystallized Benzoic Acid. In: *Industrial & Engineering Chemistry Research* 43 (2004), Nr. 21, S. 6694–6702. http://dx.doi.org/10.1021/ie049828a. – DOI 10.1021/ie049828a. – ISSN 0888–5885

[51] Lorenz, Richard: Lehrbuch der allgemeinen Chemie, von W. OSTWALD. II. Band. 2. Teil: Verwandtschaftslehre. 1. Lieferung. (Leipzig, 1896.) 5 Mark. In: *Zeitschrift fr*

anorganische Chemie 15 (1897), Nr. 1, S. 239. http://dx.doi.org/10.1002/zaac.18970150136. – DOI 10.1002/zaac.18970150136. – ISSN 0863–1778

[52] Levilain, Guillaume ; Coquerel, Gérard: Pitfalls and rewards of preferential crystallization. In: *CrystEngComm* 12 (2010), Nr. 7, S. 1983. http://dx.doi.org/10.1039/c001895c. – DOI 10.1039/c001895c

[53] Hein, Jason E. ; Cao, Blessing H. ; Viedma, Cristobal ; Kellogg, Richard M. ; Blackmond, Donna G.: Pasteur's tweezers revisited: on the mechanism of attrition-enhanced deracemization and resolution of chiral conglomerate solids. In: *Journal of the American Chemical Society* 134 (2012), Nr. 30, S. 12629–12636. http://dx.doi.org/10.1021/ja303566g. – DOI 10.1021/ja303566g

[54] Addadi, L. ; Berkovitch-Yellin, Z. ; Domb, N. ; Gati, E. ; Lahav, M. ; Leiserowitz, L.: Resolution of conglomerates by stereoselective habit modifications. In: *Nature* 296 (1982), Nr. 5852, S. 21–26. http://dx.doi.org/10.1038/296021a0. – DOI 10.1038/296021a0. – ISSN 0028–0836

[55] Addadi, L. ; Weinstein, S. ; Gati, E. ; Weissbuch, I. ; Lahav, M.: Resolution of conglomerates with the assistance of tailor-made impurities. Generality and mechanistic aspects of the "rule of reversal". A new method for assignment of absolute configuration. In: *Journal of the American Chemical Society* 104 (1982), Nr. 17, S. 4610–4617. http://dx.doi.org/10.1021/ja00381a018. – DOI 10.1021/ja00381a018

[56] Kaptein, Bernard ; Noorduin, Wim L. ; Meekes, Hugo ; van Enckevort, Willem J. P. ; Kellogg, Richard M. ; Vlieg, Elias: Attrition-enhanced deracemization of an amino acid derivative that forms an epitaxial racemic conglomerate. In: *Angewandte Chemie (International ed. in English)* 47 (2008), Nr. 38, S. 7226–7229. http://dx.doi.org/10.1002/anie.200802468. – DOI 10.1002/anie.200802468

[57] Noorduin, Wim L. ; Bode, Arno A. C. ; van der Meijden, Maarten ; Meekes, Hugo ; van Etteger, Albert F. ; van Enckevort, Willem J. P. ; Christianen, Peter C. M. ; Kaptein, Bernard ; Kellogg, Richard M. ; Rasing, Theo ; Vlieg, Elias: Complete chiral symmetry breaking of an amino acid derivative directed by circularly polarized light. In: *Nature chemistry* 1 (2009), Nr. 9, S. 729–732. http://dx.doi.org/10.1038/nchem.416. – DOI 10.1038/nchem.416

[58] Viedma, Cristóbal ; Cintas, Pedro: Homochirality beyond grinding: deracemizing chiral crystals by temperature gradient under boiling. In: *Chemical communications (Cambridge, England)* 47 (2011), Nr. 48, S. 12786–12788. http://dx.doi.org/10.1039/c1cc14857e. – DOI 10.1039/c1cc14857e

[59] Katsuno, Hiroyasu ; Uwaha, Makio: Mechanism of chirality conversion by periodic change of temperature: Role of chiral clusters. In: *Physical review. E* 93 (2016), Nr. 1, S. 013002. http://dx.doi.org/10.1103/PhysRevE.93.013002. – DOI 10.1103/PhysRevE.93.013002

[60] Belletti, Giuseppe ; Meekes, Hugo ; Rutjes, Floris P. J. T. ; Vlieg, Elias: Role of Additives during Deracemization Using Temperature Cycling. In: *Crystal growth & design* 18 (2018), Nr. 11, S. 6617–6620. http://dx.doi.org/10.1021/acs.cgd.8b00856. – DOI 10.1021/acs.cgd.8b00856. – ISSN 1528–7483

[61] Breveglieri, Francesca ; Maggioni, Giovanni M. ; Mazzotti, Marco: Deracemization of NMPA via Temperature Cycles. In: *Crystal growth & design* 18 (2018), Nr. 3, S. 1873–1881. http://dx.doi.org/10.1021/acs.cgd.7b01746. – DOI 10.1021/acs.cgd.7b01746. – ISSN 1528–7483

[62] Gonella, S. ; Levilain, G. ; Coquerel, G.: Racemizable systems crystallizing as conglomerate and spontaneous symmetry breaking. In: *Journal of Thermal Analysis and Calorimetry* 103 (2011), Nr. 1, S. 125–129. http://dx.doi.org/10.1007/s10973-010-1035-y. – DOI 10.1007/s10973–010–1035–y. – ISSN 1388–6150

[63] Noorduin, Wim L. ; Meekes, Hugo ; Bode, Arno A. C. ; van Enckevort, Willem J. P. ; Kaptein, Bernard ; Kellogg, Richard M. ; Vlieg, Elias: Explanation for the Emergence of a Single Chiral Solid State during Attrition-Enhanced Ostwald Ripening: Survival of the Fittest. In: *Crystal growth & design* 8 (2008), Nr. 5, S. 1675–1681. http://dx.doi.org/10.1021/cg701211a. – DOI 10.1021/cg701211a. – ISSN 1528–7483

[64] Iggland, Martin ; Fernández-Ronco, María P. ; Senn, Remo ; Kluge, Johannes ; Mazzotti, Marco: Complete solid state deracemization by High Pressure Homogenization. In: *Chemical Engineering Science* 111 (2014), S. 106–111. http://dx.doi.org/10.1016/j.ces.2014.02.034. – DOI 10.1016/j.ces.2014.02.034. – ISSN 00092509

[65] Cameli, Fabio ; Xiouras, Christos ; Stefanidis, Georgios D.: Intensified deracemization via rapid microwave-assisted temperature cycling. In: *CrystEngComm* 20 (2018), Nr. 21, S. 2897–2901. http://dx.doi.org/10.1039/C8CE00575C. – DOI 10.1039/C8CE00575C

[66] Kondepudi, D. K. ; Kaufman, R. J. ; Singh, N.: Chiral symmetry breaking in sodium chlorate crystallizaton. In: *Science (New York, N.Y.)* 250 (1990), Nr. 4983, S. 975–976. http://dx.doi.org/10.1126/science.250.4983.975. – DOI 10.1126/science.250.4983.975. – ISSN 0036–8075

[67] Uchin, Ratchanon ; Suwannasang, Kittisak ; Flood, Adrian E.: Model of Temperature Cycle-Induced Deracemization via Differences in Crystal Growth Rate Dispersion. In: *Chemical Engineering & Technology* 40 (2017), Nr. 7, S. 1252–1260. http://dx.doi.org/10.1002/ceat.201600746. – DOI 10.1002/ceat.201600746. – ISSN 09307516

[68] Suwannasang, Kittisak ; Coquerel, Gerard ; Rougeot, Celine ; Flood, Adrian E.: Mathematical Modeling of Chiral Symmetry Breaking due to Differences in Crystal

Growth Kinetics. In: *Chemical Engineering & Technology* 37 (2014), Nr. 8, S. 1329–1339. http://dx.doi.org/10.1002/ceat.201400056. – DOI 10.1002/ceat.201400056. – ISSN 09307516

[69] Scott Fogler, H.: *Essentials of chemical reaction engineering*. Upper Saddle River, NJ : Prentice-Hall, 2011 (Prentice Hall international series in the physical and chemical engineering sciences). – ISBN 9780132119368

[70] Fogler, H. S.: *Elements of chemical reaction engineering*. 4. ed., Pearson new internat. ed. Harlow : Pearson, 2014. – ISBN 978–129–202–616–9

[71] Levenspiel, Octave: *Chemical reaction engineering*. 3. ed. Hoboken, NJ : Wiley, 1999 http://www.loc.gov/catdir/description/wiley033/97046872.html. – ISBN 9780471254249

[72] Scott Fogler, H.: *Essentials of chemical reaction engineering*. Upper Saddle River, NJ : Prentice-Hall, 2011 (Prentice Hall international series in the physical and chemical engineering sciences). – ISBN 9780132119368

[73] Jiang, Mo ; Zhu, Zhilong ; Jimenez, Ernesto ; Papageorgiou, Charles D. ; Waetzig, Josh ; Hardy, Andrew ; Langston, Marianne ; Braatz, Richard D.: Continuous-Flow Tubular Crystallization in Slugs Spontaneously Induced by Hydrodynamics. In: *Crystal growth & design* 14 (2014), Nr. 2, S. 851–860. http://dx.doi.org/10.1021/cg401715e. – DOI 10.1021/cg401715e. – ISSN 1528–7483

[74] Iggland, Martin ; Müller, Roland ; Mazzotti, Marco: On the Effect of Initial Conditions in Viedma Ripening. In: *Crystal growth & design* 14 (2014), Nr. 5, S. 2488–2493. http://dx.doi.org/10.1021/cg500196m. – DOI 10.1021/cg500196m. – ISSN 1528–7483

[75] Lingenfelder, Magalí ; Bejarano-Villafuerte, Ángela ; van der Meijden, Maarten W. ; Kellogg, Richard M. ; Amabilino, David B.: Localized crystallization of enantiomeric organic compounds on chiral micro-patterns from various organic solutions. In: *Chemistry (Weinheim an der Bergstrasse, Germany)* 20 (2014), Nr. 33, S. 10466–10474. http://dx.doi.org/10.1002/chem.201303062. – DOI 10.1002/chem.201303062

[76] Noorduin, Wim L. ; Meekes, Hugo ; van Enckevort, Willem J. P. ; Millemaggi, Alessia ; Leeman, Michel ; Kaptein, Bernard ; Kellogg, Richard M. ; Vlieg, Elias: Complete deracemization by attrition-enhanced ostwald ripening elucidated. In: *Angewandte Chemie (International ed. in English)* 47 (2008), Nr. 34, S. 6445–6447. http://dx.doi.org/10.1002/anie.200801846. – DOI 10.1002/anie.200801846

[77] Köllges, Till ; Vetter, Thomas: Design and Performance Assessment of Continuous Crystallization Processes Resolving Racemic Conglomerates. In: *Crystal growth & design* 18 (2018), Nr. 3, S. 1686–1696. http://dx.doi.org/10.1021/acs.cgd.7b01618. – DOI 10.1021/acs.cgd.7b01618. – ISSN 1528–7483

[78] Sigma-Aldrich (Hrsg.): *Sicherheitsdatenblatt: gemäß Verordnung (EG) Nr. 1907/2006.* `http://www.merckmillipore.com/AT/de/product/msds/MDA_CHEM-803282?Origin=PDP`. Version: 01.08.2019

[79] Lide, David R. (Hrsg.): *CRC handbook of chemistry and physics: A ready-reference book of chemical and physical data.* 87. ed., 2006-2007. Boca Raton, Fla. : CRC Taylor & Francis, 2006. – ISBN 0849304873

List of Figures

List of Tables